Inorg. Chem. **2008**, *47*, 8143−8158

Anion Influence on the Structure and Magnetic Properties of a Series of Multidimensional Pyrimidine-2-carboxylato-Bridged Copper(II) Complexes

José Suárez-Varela,[†] Antonio J. Mota,[†] Hakima Aouryaghal,[‡] Joan Cano,*[,§] A. Rodríguez-Diéguez,[†] Dominique Luneau,[||] and Enrique Colacio*[,†]

Departamento de Química Inorgánica, Universidad de Granada, Av. Fuentenueva S/N, 18071 Granada, Spain, Departement de Chimie, Université Abdelmalek Essaadi, Faculté des Sciences, P.O. 2121, Tétouan, Marocco, Departament de Química Inorgànica and Institut de Recerca de Química Teòrica i Computacional (IQTC), Universitat de Barcelona, Av. Diagonal 647, 08027 Barcelona, Spain, and Laboratoire des Multimateriaux et Interfaces, (UMR 5615), Université ClaudeBernard Lyon-1, 69622 Villeurbanne cedex, France

Received April 11, 2008

Seven new polynuclear copper(II) complexes of formula [Cu(μ-pymca)$_2$] (**1**) (pymca$^-$ = pyrimidine-2-carboxylato), [Cu(μ-pymca)Br] (**2**), [Cu(μ-pymca)Cl] (**3**), [Cu(μ-pymca)(SCN)(H$_2$O)]·4H$_2$O (**4**), [Cu(μ-pymca)N$_3$] (**5**), [Cu$_2$($\mu_{1,5}$-dca)$_2$(pymca)$_2$] (**6**) (dca = dicyanamide), and K{[μ-Au(CN)$_2$]$_2$[(Cu(NH$_3$)$_2$)$_2$(μ-pymca)]}[Au(CN)$_2$]$_2$ (**7**) have been synthesized by reactions of K-pymca with copper(II) ions in the presence of different counteranions. Compound **1** is a linear neutral chain with a carboxylato bridging ligand in a syn−anti coordination mode, whereas complexes **2** and **3** consist of cationic linear chains with cis and trans bis(chelating) pymca bridging ligands. Complex **4** adopts a helical pymca-bridged chain structure. In complex **5**, zigzag pymca-bridged chains are connected by double end-on azide bridging ligands to afford a unique honeycomb layer structure. Complex **6** is a centrosymmetric dinuclear system with double $\mu_{1,5}$-dicyanamide bridging ligands and pymca end-cap ligands. Complex **7** is made of pymca-bridged dinuclear [Cu(NH$_3$)$_2$(μ-pymca)Cu(NH$_3$)$_2$]$^{3+}$ units connected by [Au(CN)$_2$]$^-$ anions to four other dinuclear units, giving rise to cationic (4,4) rectangular nets, which are linked by aurophilic interactions to afford a singular 3D network. Variable-temperature magnetic susceptibility measurements show that complex **1** exhibits a very weak antiferromagnetic coupling through the syn−anti (equatorial−axial) carboxylate bridge (J = −0.57 cm^{-1}), whereas complexes **2**−**4** and **7** exhibit weak to strong antiferromagnetic couplings through the bis(chelating) pymca bridging ligand (J = −17.5−276.1 cm^{-1}). Quantum Monte Carlo methods have been used to analyze the experimental magnetic data for **5**, leading to an antiferromagnetic coupling (J = −34 cm^{-1}) through the pymca ligand and to a ferromagnetic coupling (J = 71 cm^{-1}) through the azide bridging ligands. Complex **6** exhibits a very weak antiferromagnetic coupling through the dicyanamide bridging ligands (J = −5.1 cm^{-1}). The magnitudes of the magnetic couplings in complexes **2**−**5** have been explained on the basis of the overlapping between magnetic orbitals and DFT theoretical calculations.

Introduction

During the two past decades, crystal engineering techniques have been widely used for the design and synthesis of coordination framework materials with specific solid-state properties, such as electrical conductivity, molecular magnetism, molecular absorption, catalysis, ion-exchange, and so forth.[1] Among them, molecule-based magnetic materials[2] have been commonly prepared through a bottom-up approach, connecting paramagnetic transition metal ions with appropriate bridging ligands. The information encoded in the transition metal and organic ligands directs the self-assembly of these building blocks in a programmed way. The metal ions are the source of magnetic moments, whereas the bridging ligands allow for the magnetic exchange coupling between the magnetic centers. Only a few polyatomic

* Authors to whom correspondence should be addressed. E-mail: ecolacio@ugr.es (E.C.).
[†] Universidad de Granada.
[‡] Université Abdelmalek Essaadi.
[§] Universitat de Barcelona.
[||] Université ClaudeBernard Lyon-1.

10.1021/ic800625w CCC: $40.75
Published on Web 08/13/2008

bridging ligands have been shown to be able to mediate strong magnetic coupling between transition metal ions,[2a] and consequently there still exists great interest in the search for new bridging ligands which can generate magnetic materials with structural and topological novelty and intriguing magnetic properties. Recently, we succeeded in obtaining by the hydrothermal reaction of 2-cyanopyrimidine and either $CoCl_2 \cdot 6H_2O$ or $FeCl_2 \cdot 4H_2O$ honeycomb-layered metal complexes $[M_2(\mu\text{-pymca})_3]OH \cdot H_2O$ containing a new bis-bidentate ligand (pymca = pyrimidine-2-carboxylato), which was generated *in situ* from the hydrolysis of 2-cyanopyrimidine.[3] The pymca ligand, which can be considered as an intermediate case between bipyrimidine and oxalato, is able to transmit efficiently antiferromagnetic interactions between metal ions. After this pioneering work and by using the same synthetic strategy, Eddaoudi et al.[4] and Gao et al.[5] have succeeded in preparing two zeolite-like metal-organic frameworks constructed from pymca and Cd(II) ions, which exhibit interesting adsorption properties. Because pymca offers donor atom sets and charge-balance requirements other than those of bipyrimidine and oxalate and because it possesses great potential for the design of new functional magnetic materials based on coordination polymer networks, we decided to undertake the synthesis of pymca and to explore its coordinative ability against metal ions using mild conditions. In this paper, we report the syntheses, structures, and magnetic properties of a series of Cu(II)-pymca complexes, which show wide structural diversity: (a) dinuclear $[Cu_2(\mu_{1,5}\text{-dca})_2(pymca)_2]$, (b) linear $[Cu(\mu\text{-pymca})_2]$ and helical $[Cu(\mu\text{-pymca})(SCN)(H_2O)] \cdot 4H_2O$ chains, (c) (4,4) rectangular grid $[Cu(\mu\text{-pymca})Cl]$ and $[Cu(\mu\text{-pymca})Br]$, (d) (6,3) honeycomb layer $[[Cu(\mu\text{-pymca})N_3]$, and (e) 3D network $K\{[\mu\text{-}Au(CN)_2]_2[(Cu(NH_3)_2)_2(\mu\text{-pymca})]\}[Au(CN)_2]_2$. It is of interest that the nature of the copper(II) counterions has an important influence on the structure of the pymca-bridged copper(II) assemblies **1**−**7**. Nowadays, the study of the influence of the anionic counterion on the final structure is an area of great research interest and activity.[6]

Experimental Section

All analytical reagents were purchased from commercial sources and used without further purification. 2-Cyanopyrimidine was prepared according to a previously described procedure.[7]

Preparation of the Compounds. H-pymca. A suspension of 2-cyanopyrimidine (2 g, 19 mmol) in 50 mL of water was treated with KOH (2,24 g, 40 mmol) and the mixture refluxed for 2 h. The resulting solution was neutralized with HCl 2N, and then the solvent was removed in a vacuum. The obtained crude product was treated with CH_2Cl_2; the KCl was filtered off and the filtrate concentrated to afford the H-pymca acid in a yield of 40%. ^{1}H NMR (δ): H_3 and H_5 (8.76, doublet), H_4 (7.44, triplet). ^{13}C NMR (δ): C_4 (122.7), C_3 and C_5 (157.8), C_1 (160.7), C_7OOH (170.4).

$Cu(pymca)_2$ (1). The reaction in a water/methanol mixture (50:50, 30 mL) of the K-pymca salt, generated in situ from H-pymca (0.012 g, 0.1 mmol) and KOH (0.006 g, 0.1 mmol), and $Cu(NO_3)_2 \cdot 4H_2O$ (0.013 g, 0.05 mmol) in a 2:1 molar ratio led to a blue solution, which kept at room temperature for several days gave rise to blue crystals of complex **1**, which were filtered off and air-dried. Alternatively, compound **1** can be obtained from the reaction between 2-cyanopyrimidine and $Cu(Ac)_2 \cdot H_2O$ in MeOH at reflux for 2 h. Yield: *ca* 60%. Anal. calcd for $C_{10}H_6N_4O_4Cu$: C, 38.78; H, 1.95; N, 18.09. Found: C, 38.90; H, 2.05; N, 17.97. IR (KBr, cm^{-1}): 3080, ν(CH); 1641, $\nu(COO)_{as}$; 1597, ν(C=C); 1398, $\nu(COO)_s$.

[Cu(μ-pymca)Br] (2). The reaction of an aqueous solution (20 mL) of the K-pymca salt, generated in situ from H-pymca (0.031 g, 0.25 mmol) and KOH (0.014 g, 0.25 mmol), and $CuBr_2$ (0.167 g, 0.75 mmol) in a 1:3 molar ratio afforded a green-blue solution, which kept at room temperature for a week led to green crystals of **2**, which were filtered off and air-dried. Yield: *ca* 52%. Anal. calcd

(1) (a) Blake, A. J.; Champness, N. R.; Hubberstey, P.; Li, W. S.; Withersby, M. A.; Schröder, M. *Coord. Chem. Rev.* **1999**, *183*, 117. (b) Zaworotko, M. J. *Angew. Chem., Int. Ed. Engl.* **2000**, *39*, 3052. (c) Moulton, B.; Zaworotko, M. J. *Chem. Rev.* **2001**, *101*, 1629. (d) Oxtoby, S. A.; Champness, N. R. *Coord. Chem. Rev.* **2003**, *246*, 145. (e) Eddaoudi, M.; Moler, D. B.; Li, H.; Chen, B.; Reinecke, T. M.; O'Keeffe, M.; Yaghi, O. *Acc. Chem. Res.* **2001**, *34*, 319. (f) Batten, S. R. *Curr. Opin. Solid State Mater. Sci.* **2001**, *5*, 107. (g) Janiak, C. *Dalton Trans.* **2003**, 2781. (h) Kitagawa, S.; Kitaura, R.; Noro, S.-I. *Angew. Chem., Int. Ed.* **2004**, *43*, 2334. (i) Rowsell, J. L.; Yaghi, O. M. *Microporous Mesoporous Mater.* **2004**, *73*, 3. (j) Ockwing, N. W.; Delgado-Friedirchs, O.; O'Keefe, M.; Yaghi, O. M. *Acc. Chem. Res.* **2005**, *38*, 178. (k) Plecnik, C. E.; Lin, S. M.; Shore, S. G. *Acc. Chem. Res.* **2003**, *36*, 449. (l) Bünzli, J. C. G. *Acc. Chem. Res.* **2006**, *39*, 53. (m) Kitagawa, S.; Uemura, K. *Chem. Soc. Rev.* **2005**, *34*, 109. (n) Evans, R. C.; Douglas, P.; Winscom, C. J. *Coord. Chem. Rev.* **2006**, *250*, 2093. (o) Ward, M. D. *Coord. Chem. Rev.* **2007**, *251*, 1663. (p) Foxman, B. M.; Ward, M. D. *MRS Bull.* **2007**, *32* (7). (q) Robin, A. Y.; Fromm, K. M. *Coord. Chem. Rev.* **2006**, *250*, 2127.

(2) (a) *Magnetism: Molecules to Materials*; Miller, J. S.; Drillon, M., Eds.; Wiley-VCH: Weinheim, Germany, 2005; Vol. I-V. (b) Khan, O. *Adv. Inorg. Chem.* **1995**, *43*, 179. (c) Miller, J. S.; Epstein, A. *MRS Bull.* **2000**, *25*, 11. (d) Khan, O. *Acc. Chem. Res.* **2000**, *33*, 647. (e) Verdaguer, M.; Bleuzen, A.; Marvaud, V.; Vaissermann, J.; Seuleiman, M.; Desplanches, C.; Scuiller, A.; Train, C.; Garde, R.; Gelly, G.; Lomenech, C.; Rosenman, I.; Veillet, P.; Cartier, C.; Villain, F. *Coord. Chem. Rev.* **1999**, *190*, 1023. (f) Ohba, M.; Okawa, K. *Coord. Chem. Rev.* **2000**, *198*, 313. (g) Batten, S. R.; Murray, K. S. *Coord. Chem. Rev.* **2003**, *246*, 103. (h) Sorai, M.; Nakano, M.; Miyazaki, Y. *Chem. Rev.* **2006**, *106*, 976. (i) Przychodsen; Korzeniak, T.; Podgajni, R.; Sieklucka, B. *Coord. Chem. Rev.* **2006**, *250*, 2234. (j) Beltran, L. M.; Long, J. R. *Acc. Chem. Res.* **2005**, *38*, 325. (k) Aromí, G.; Brechin, E. K. *Struct. Bonding (Berlin)* **2006**, *122*, 1. (l) Rebilly, J.-N.; Rebilly, T.; Mallah, *Struct. Bonding (Berlin)* **2006**, *122*, 103. (m) Cornia, A.; Costantino, A. F.; Zobbi, L.; Caneshi, A.; Gatteschi, D.; Mannini, M.; Sessoli, R. *Struct. Bonding (Berlin)* **2006**, *122*, 133. (n) Gatteschi, D.; Sessoli, Villain, J. *Molecular Nanomagnets*; Oxford University Press: Oxford, U.K., 2006. (o) Lescouëzec, R.; Toma, L. M.; Vaissermann, J.; Verdaguer, M.; Delgado, F. S.; Ruiz-Pérez, C.; Lloret, F.; Julve, M. *Coord. Chem. Rev.* **2005**, *249*, 2691. (p) Coulon, C.; Miyasaka, H.; Clérac, R. *Struct. Bonding (Berlin)* **2006**, *122*, 163. (q) Bernot, K.; Bogani, L.; Caneschi, A.; Gatteschi, D.; Sessoli, R. *J. Am. Chem. Soc.* **2006**, *128*, 7947. (r) Real, J. A.; Gaspar, A. B.; Niel, V.; Muñoz, M. C. *Coord. Chem. Rev.* **2003**, *236*, 121. (s) García, Y.; Niel, V.; Muñoz, M. C.; Real, J. A. *Top. Curr. Chem.* **2004**, *233*, 229.

(3) Rodríguez-Diéguez, A.; Cano, J.; Kivekäs, R.; Debdoubi, A.; Colacio, E. *Inorg. Chem.* **2007**, *46*, 2503.

(4) Sava, D. F.; Kravtsov, V. C.; Nouar, F.; Wojtas, L.; Eubank, J. F.; Eddaoudi, M. *J. Am. Chem. Soc.* **2008**, *130*, 3768.

(5) Zhang, J.-Y.; Cheng, A.-L.; Yue, Q.; Sun, W. W.; Gao, E.-Q. *Chem. Commun.* **2008**, 847.

(6) (a) Khlobysov, A. N.; Blake, A. J.; Champness, N. R.; Lemenovski, D. A.; Majouga, A. G.; Zyk, N. V.; Schröeder, M. *Coord. Chem. Rev.* **2001**, *222*, 155. (b) Hannon, M. J.; Painting, C. L.; Plummer, E. A.; Childs, L. J.; Alcock, N. W. *Chem.—Eur. J.* **2002**, *8*, 2225. (c) Díaz, P.; Benet-Buchholz, J.; Vilar, R.; White, A. P. J. *Inorg. Chem.* **2006**, *45*, 1617. (d) Bisiwas, C.; Mukherjee, P.; Drew, M. G. B.; Gómez-García, C. J.; Clemente-Juan, J. M.; Ghosh, A. *Inorg. Chem.* **2007**, *46*, 10771. (e) Mukherjee, P.; Drew, M. G. B.; Estrader, M.; Díaz, C.; Gosh, A. *Inorg. Chim. Acta* **2008**, *361*, 161. (f) Custelcean, R. *Chem. Commum.* **2006**, 295.

(7) Case, F. H.; Koft, E. *J. Am. Chem. Soc.* **1959**, *81*, 905.

Table 1. Crystallographic Data and Structural Refinement Details for Compounds **1**−**7**

compound	**1**	**2**	**3**	**4**	**5**	**6**	**7**
chemical formula	$C_{10}H_6CuN_4O_4$	$C_5H_3BrCuN_2O_2$	$C_5H_3ClCuN_2O_2$	$C_6H_3CuN_3O_2S\cdot 3.33H_2O$	$C_5H_3CuN_5O_2$	$C_7H_5CuN_5O_3$	$C_{13}H_3Au_4Cu_2KN_{14}O_2$
M/gmol^{-1}	309.73	266.54	222.08	304.71	228.67	270.70	1341.35
T (K)	293(2)	293(2)	298(2)	293(2)	293(2)	293(2)	293(2)
λ/Å	0.71073	0.71073	0.71073	0.71073	0.71073	0.71073	0.71073
cryst syst	monoclinic	orthorhombic	orthorhombic	trigonal	monoclinic	triclinic	monoclinic
space group	$P21/c$	$Pmc21$	$Pbcm$	$R\bar{3}$	$C2/c$	$P\bar{1}$	$C2/c$
a/Å	5.1422(5)	5.2929(8)	6.5488(6)	21.5359(10)	9.7896(8)	6.5203(13)	19.731(5)
b/Å	13.2586(11)	6.7384(10)	9.4281(8)	21.5359(10)	11.6751(10)	8.1470(16)	15.198(4)
c/Å	7.6747(7)	9.8478(14)	10.6417(9)	13.2232(13)	13.2753(11)	9.998(2)	9.498(2)
α/deg	90.00	90.00	90.00	90.00	90.00	84.71(3)	90.00
β/deg	93.961(2)	90.00	90.00	90.00	100.925(10)	72.64(3)	95.615(4)
γ/deg	90.00	90.00	90.00	120.00	90.00	67.20(3)	90.00
V/Å^3	522.00(8)	351.23(9)	657.05(10)	5311.2(6)	1489.8(2)	467.16(16)	2834.6(12)
Z	2	2	4	18	8	2	4
ρ (g cm^{-3})	1.971	2.520	2.245	1.677	2.039	1.924	3.143
μ (mm^{-1})	2.110	8.737	3.666	2.039	2.901	2.337	22.282
GOF on F^2	1.072	1.097	1.135	1.036	1.063	1.047	1.029
R1 [$I > 2\sigma(I)$]	0.0258	0.0270	0.0249	0.0584	0.0341	0.0239	0.0476
wR2 [$I > 2\sigma(I)$]	0.0725	0.0745	0.0745	0.1660	0.0796	0.0639	0.1274

for $C_5H_3N_2O_2CuBr$: C, 22.53; H, 1.13; N, 10.51. Found: C, 22.78; H, 1.32; N, 10.05. IR (KBr, cm^{-1}): 3098, 3074, ν(CH); 1629, $\nu(COO)_{as}$; 1605, ν(C═C); 1392, $\nu(COO)_s$.

[Cu(μ-pymca)Cl] (3). This compound was prepared as blue crystals by following the same method as for **2**, but using $CuCl_2\cdot 2H_2O$ (0.127 g, 0.75 mmol) instead of $CuBr_2$. Yield: *ca* 57%. Anal. calcd for $C_5H_3N_2O_2CuCl$: C, 27.04; H, 1.36; N, 12.61. Found: C, 27.42; H, 1.62; N, 12.15. IR (KBr, cm^{-1}): 3106, 3079, ν(CH); 1641, $\nu(COO)_{as}$; 1609, ν(C═C); 1368, $\nu(COO)_s$.

[Cu(μ-pymca)(SCN)(H_2O)]·$4H_2O$ (4). To the blue aqueous solution (20 mL) obtained from K-pymca salt, generated in situ from H-pymca (0.031 g, 0.25 mmol) and KOH (0.014 g, 0.25 mmol), and $CuCl_2\cdot 2H_2O$ (0.127 g, 0.75 mmol) was added with stirring a water solution (10 mL) of KSCN (0.072 g, 0.75 mmol). The resulting blue solution was allowed to stand at room temperature for several days, whereupon blue crystals of **3** formed, which were filtered off and air-dried. Yield: *ca* 62%. Anal. calcd for $C_6H_{11}N_3O_6CuS$: C, 22.75; H, 3.50; N, 13.26. Found: C, 22.81; H, 3.80; N, 12.95. IR (KBr, cm^{-1}): 3416, ν(OH); 3098, 3074, ν(CH); 2104, ν(C≡N); 1669, ν(OH); 1654, $\nu(COO)_{as}$; 1598, ν(C═C); 1384, $\nu(COO)_s$.

Compounds [Cu(μ-pymca)N_3] (**5**) and [Cu_2(μ-dca)$_2$(pymca)$_2$] (**6**) were prepared by following the same method as for (**4**), but using NaN_3 (0.049 g, 0.75 mmol) and Na(dca) (0.066 g, 0.75 mmol) instead of KSCN, respectively.

[Cu(μ-pymca)N_3] (5). Yield: *ca* 37%. Anal. calcd for $C_5H_3N_5O_2Cu$: C, 26.26; H, 1.32; N, 30.62. Found: C, 26.45; H, 1.52; N, 30.18. IR (KBr, cm^{-1}): 3108, 3084, ν(CH); 2069, 2043, ν(N3); 1656, $\nu(COO)_{as}$; 1592, ν(C═C); 1367, $\nu(COO)_s$.

[Cu_2(μ-dca)$_2$(pymca)$_2$] (6). Yield: *ca* 46%. Anal. calcd for $C_7H_3N_8O_2Cu$: C, 28.53; H, 1.03; N, 38.02. Found: C, 28.70; H, 1.22; N, 38.18. IR (KBr, cm^{-1}): 3092, 3067, ν(CH); 2422, 2335, 2268, 2197, ν(C≡N); 1656, $\nu(COO)_{as}$; 1592, ν(C═C); 1367, $\nu(COO)_s$.

K{[μ-$(CN)_2$]$_2$[($Cu(NH_3)_2$)$_2$(μ-pymca)]}[$Au(CN)_2$]$_2$ (7). To 20 mL of water were successively added pyrimidin-2-carboxylic acid (0.0062 g, 0.05 mmol) and $CuCl_2\cdot 2H_2O$ (0.017 g, 0.1 mmol). The mixture was stirred for 5 min, and then 10 mL of concentrated ammonia was added. A solution of K[$Au(CN)_2$] (0.058 g, 0.2 mmol) in 10 mL of water was then added, and the resulting solution was filtered. After 24 h, blue crystals of **7** appeared, which were collected by filtration and dried in the air. Yield: *ca* 54%. Anal. calcd for $C_{13}H_{15}N_{14}O_2Cu_2Au_4$: C, 11.54; H, 1.11; N, 14.49. Found: C, 11.82; H, 1.28; N, 14.35. IR (KBr, cm^{-1}): 3360, 3276, 3173, ν(NH); 3062, ν(CH); 2175, 2137, ν(C≡N); 1649, $\nu(COO)_{as}$; 1583, ν(C═C); 1374, $\nu(COO)_s$.

Physical Measurements. Elemental analyses were carried out at the "Centro de Instrumentación Científica" (University of Granada) on a Fisons-Carlo Erba analyzer model EA 1108. The IR spectra on powdered samples were recorded with a ThermoNicolet IR200FTIR by using KBr pellets. Magnetization and variable-temperature (1.9−300 K) magnetic susceptibility measurements on polycrystalline samples were carried out with a Quantum Design SQUID operating at a field of 0.5 T. The experimental susceptibilities were corrected for the diamagnetism of the constituent atoms by using Pascal's tables. It should be noted at this point that the powder X-ray diffractograms of the bulk samples used for the magnetic measurements match well those calculated from the crystal structures (see Figure S1, Supporting Information).

X-Ray Crystallography. Single-crystal data collections for **1**−**7** were carried out on a Bruker Smart Apex diffractometer using graphite monochromatized Mo Kα radiation. The structures were solved by direct methods and refined on F^2 by the SHELXL97 program.[8] Hydrogen atoms bonded to water molecules could not be reliably positioned, but the rest of the hydrogen atoms were treated as riding atoms using the SHELX97 default parameters. A summary of the crystallographic data and structure refinements is given in Table 1.

Computational Details. All theoretical calculations were carried out with the hybrid B3LYP method,[9] as implemented in the Gaussian 03 program.[10] A quadratic convergence method was employed in the self-consistent field process.[11] The triple-ζ-quality basis set proposed by Ahlrichs and co-workers was used for all atoms.[12] The calculations were performed on the complexes built from the experimental geometries. More detailed information about the models can be found in the discussion of the results. The electronic configurations used as starting points were created using Jaguar 6.0 software.[13] The approach that we used herein to determine the exchange coupling constants for polynuclear complexes has been described in detail elsewhere.[14]

(8) Sheldrick, G. M. *SHELX 97*; University of Göttingen: Göttingen, Germany, 1997.
(9) (a) Becke, A. D. *Phys. Rev. A: At., Mol., Opt. Phys.* **1988**, *38*, 3098. (b) Lee, C. T.; Yang, W. T.; Parr, R. G. *Phys. Rev. B: Condens. Matter Mater. Phys.* **1988**, *37*, 785. (c) Becke, A. D. *J. Chem. Phys.* **1993**, *98*, 5648.

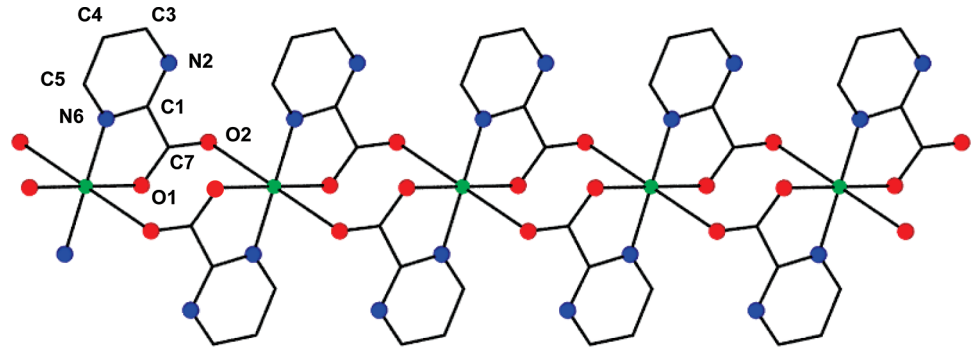

Figure 1. Perspective view of the chain structure of **1**.

Results and Discussion

The reaction of K-pymca, generated *in situ* from 2-carboxypyrimidine and KOH, with copper(II) salts was shown to be strongly dependent on the anion present in the reaction solution and the metal-to-ligand molar ratio. When either 1:1 or 1:2 metal-to-ligand molar ratios were used, only the neutral complex [Cu(pymca)$_2$] (**1**) was obtained. However, in the presence of an excess of copper salt (3:1 metal-to-ligand molar ratio), the products were those of the type [Cu(pymca)X] (X = Br^- (**2**), Cl^- (**3**), SCN^- (**4**), N_3^- (**5**), and $[N(CN)_2]^-$ (**6**)). Compounds **4**, **5**, and **6** were actually prepared from the methatetical substitution in a solution of **2** of the chloride by the corresponding anion. Although there is not any experimental evidence supporting the mechanism, we tentatively propose that the formation of **7** might occur in two steps. First, the reaction of H-pymca with an excess of $CuCl_2 \cdot 2H_2O$ (2:1 metal-to-ligand molar ratio) in aqueous ammonia would lead to the *in situ* generated dinuclear cation $[(Cu(NH_3)_2S_2(\mu\text{-pymca})Cu(NH_3)_2S_2]^{3+}$ (S = NH_3 or H_2O). Second, the peripheral S ligands would be replaced by $[Au(CN)_2]^-$ anions, leading to complex **7**. The ammonia plays an important role during the reaction; as it helps to dissolve reagents and products, it acts as a base to deprotonate the H-pymca ligand, and it coordinates temporarily or permanently to copper(II) ions.

Crystal Structures. The structure of **1** is made of planar [Cu(pymca)$_2$] units connected by weak Cu−O axial interactions to afford linear chains parallel to the *a* axis (Figure 1).

Cu(II) ions, which lie on a center of symmetry, exhibit a 4 + 2 CuO_4N_2 coordination polyhedron with tetragonally distorted octahedral geometry. The equatorial positions at about 2 Å are occupied by two nitrogen atoms and two oxygen atoms belonging to two pymca bridging ligands, which adopt a trans-planar configuration. Two carboxylate oxygen atoms, O2, are situated in axial positions at a longer distance of 2.729(2) Å. Neighboring [Cu(pymca)$_2$] units are held together by a pair of complementary weak Cu−O2 interactions, which ultimately lead to the chain structure with syn−anti carboxylate bridges. The Cu···Cu distance along the chain is 5.142(1) Å, whereas the shortest Cu···Cu interchain distance is 7.660(1) Å.

The structure of **2** consists of cationic linear chains $[Cu(pymca)]_n^{n+}$ running along the *a* axis and bromide anions that weakly connect the chains to afford sheets parallel to the *ac* plane (Figure 2).

Within each chain, copper(II) ions, which are bridged by bisbidentate pymca ligands, exhibit a 4 + 2 $CuN_2O_2Br_2$ chromophore with tetragonally distorted octahedral geometry. Four short bonds of about 2 Å are formed with two nitrogen atoms and two oxygen atoms belonging to two pymca bridging ligands, which adopt a cis-planar configuration. The axial positions are occupied by the bromine ligands at longer distances of 2.788(1) and 2.792 Å (Figure 2, left). N−Cu−O angles markedly differ from 90° as a consequence of the small bite angle of the pymca ligand (N−Cu−O = 83.69(10) Å). It should be noted that each chain made of $[Cu(pymca)]^+$ units has two planes of symmetry orthogonal to the plane of the pymca ligands, one along the Cu−Br−Cu-Br line and the other one along the $C_{Ph}-C_{COO}$ bond, and therefore the chains are strictly planar with the aromatic ring displaying the same orientation with respect to the chain. Neighboring chains are turned to each other by 52.8°, and consequently sheets are not planar but corrugated. The bromide bridging anions are at the peaks and valleys of the sheets (Figure 2, right). Within each sheet, the Cu···Cu distances across the pymca and bromide bridging ligands are 5.293(1) and 4.924 (1) Å, respectively, with a Cu−Br−Cu angle of 123.87(1). Corrugated sheets running in the *ac* plane stack along the *b*

(10) Frisch, M. J.; Trucks, G. W.; Schlegel, H. B.; Scuseria, G. E.; Robb, M. A.; Cheeseman, J. R.; Montgomery, J. J. A.; Vreven, T.; Kudin, K.; Burant, J. C.; Millam, J. M.; Iyengar, S. S.; Tomasi, J.; Barone, V.; Mennucci, B.; Cossi, M.; Scalmani, G.; Rega, N.; Petersson, G. A.; Nakatsuji, H.; Hada, M.; Ehara, M.; Toyota, K.; Fukuda, R.; Hasegawa, J.; Ishida, M.; Nakajima, T.; Honda, Y.; Kitao, O.; Nakai, H.; Klene, M.; Li, X.; Knox, J. E.; Hratchian, H. P.; Cross, J. B.; Bakken, V.; Adamo, C.; Jaramillo, J.; Gomperts, R.; Stratmann, R. E.; Yazyev, O.; Austin, A. J.; Cammi, R.; Pomelli, C.; Ochterski, J. W.; Ayala, P.; Morokuma, K.; Voth, G. A.; Salvador, P.; Dannenberg, J. J.; Zakrzewski, V. G.; Dapprich, S.; Daniels, A. D.; Strain, M. C.; Farkas, O.; Malick, D. K.; Rabuck, A. D.; Raghavachari, K.; Foresman, J. B.; Ortiz, J. V.; Cui, Q.; Baboul, A.; Clifford, S.; Cioslowski, J.; Stefanov, B. B.; Liu, G.; Liashenko, A.; Piskorz, P.; Komaromi, I.; Martin, L.; Fox, D. J.; Keith, T.:; Al-Laham, M. A.; Peng, C. Y.; Nanayakkara, A.; Challacombe, M.; Gill, P. M. W.; Johnson, B.; Chen, W.; Wong, M. W.; Gonzalez, C.; Pople, J. A. *Gaussian 03*, revision C.02; Gaussian, Inc.: Wallingford, CT, 2004.
(11) Bacskay, G. B. *Chem. Phys.* **1981**, *61*, 385.
(12) Schäfer, A.; Huber, C.; Ahlrichs, R. J. *Chem. Phys.* **1994**, *100*, 5829.
(13) *Jaguar 6.0*; Schrödinger, Inc.: Portland, 2005.
(14) (a) Ruiz, E.; Cano, J.; Alvarez, S.; Alemany, P. *J. Comput. Chem.* **1999**, *20*, 1391. (b) Ruiz, E.; Alvarez, S.; Rodríguez-Fortea, A.; Alemany, P.; Puoillon, Y.; Massobrio, C. In *Magnetism: Molecules to Materials*; Miller, J. S., Drillon, M., Eds.; Wiley-VCH: Weinheim, Germany, 2001; Vol. *II*, p 5572. (c) Ruiz, E.; Rodriguez-Fortea, A.; Cano, J.; Alvarez, S.; Alemany, P. *J. Comput. Chem.* **2003**, *24*, 982. (d) Ruiz, E.; Alvarez, S.; Cano, J.; Polo, V. *J. Chem. Phys.* **2005**, *123*, 164110.

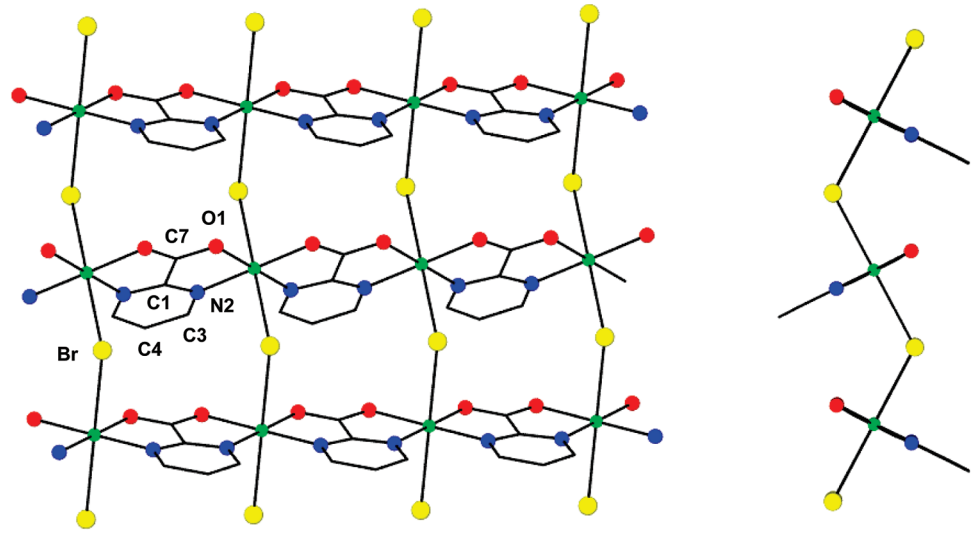

Figure 2. Perspective view of the 2D layer structure of **2** in the *ac* plane (left). View of the layer down the *a* axis (right).

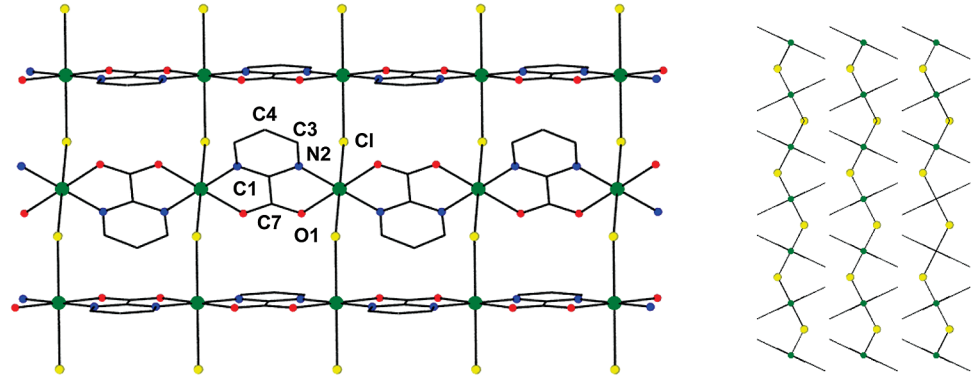

Figure 3. Perspective view of the 2D layer structure of **3** in the *bc* plane (left). View of the layers down the *c* axis (right).

axis as a result of the bifurcated C−H····Br interactions involving the bromide anion on a sheet and the C3−H groups of the same $Cu(pymca)_2$ unit on a neighboring sheet with a C···Br separation of 3.615(2) and 3.696(2) Å. The pyrimidine aromatic rings are oriented in an alternated manner above and below each sheet, leading to alternated CH···Br interlayer interactions, the shortest Cu···Cu interlayer separation being 6.738 Å.

The structure of **3** is similar to that of **2** and consists of cationic linear chains $[Cu(pymca)]_n^{n+}$ running along the *c* axis and chloride anions connecting the chains to afford a corrugated 2D network in the *bc* plane (Figure 3).

As in **2**, the mean planes containing the pymca and Cu(II) ions on neighboring chains form a dihedral angle of 51.4°, leading to sheet corrugation. Owing to the center of symmetry located on each copper(II) ion, the pymca-containing chains are strictly planar, with the aromatic ring displaying a zigzag distribution along the linear chain. Within each sheet, the Cu····Cu distance across the pymca and chloride bridging ligands are 5.321(1) and 4.714(1) Å, respectively, with a Cu−Cl−Cu angle of 126.01(1)°. Corrugated sheets running in the *bc* plane stack along the *a* axis as a result of the bifurcated Cl···H−C interactions involving the chloride anion of a sheet and two C3−H groups of two different $[Cu(pymca)_2]$ units of the neighboring sheet, with a C−Cl distance of 3.521 Å. These interactions alternate below and above each sheet, leading to a 3D network.

The main differences between both structures are (a) the disposition of the pymca ligands around the copper(II) ion, which is cis in **2** (pymca ligands along the chain are related by a plane of symmetry) and trans in **3** (pymca ligands along the chain are related by a center of symmetry), and (b) in spite of the greater size of the bromide anion compared to the chloride anion, Cu−Cl and Cu−Br distances are similar, thus indicating that the Cu−Br interaction is stronger than the Cu−Cl one.

The structure of $[Cu(\mu\text{-pymca})(SCN)(H_2O)]\cdot 4H_2O$, **4**, consists of neutral helical pymca-bridged copper(II) chains (extended along a 3-fold screw axis) and water molecules, which are held together by hydrogen bonds (Figure 4).

The copper atom has a distorted octahedral *mer*-CuN_3O_3 chromophore. Four short bonds of about 2 Å are formed in the equatorial plane with two pyrimidyl nitrogen atoms belonging to two bridging pymca ligands, one thiocyanate nitrogen atom and one carboxylate oxygen atom also belonging to one of the pymca ligands. The axial positions at longer distances are occupied by the carboxylato oxygen atom of the other pymca ligand and the oxygen atom of the water molecule. The dihedral angle between the mean planes

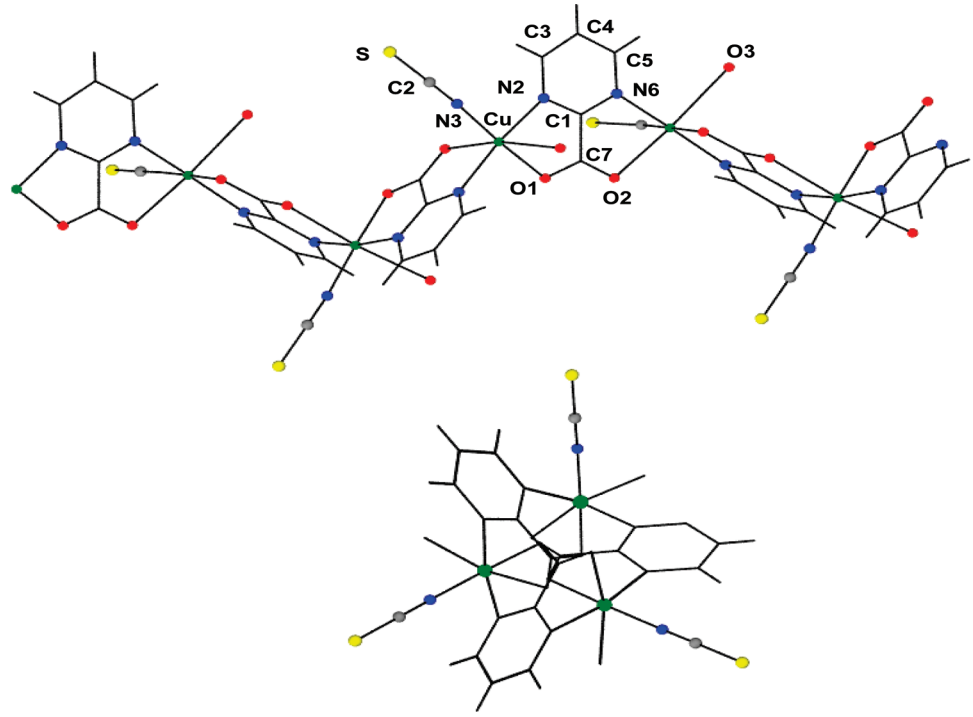

Figure 4. Zig-zag chain structure of **4** (top). View along the *c* axis of the chain of **4** (bottom).

of two neighboring ligands along the chain is 88.15(1)°, while the Cu···Cu···Cu angle is 117.6(1)°. Chains are linked by hydrogen-bond interactions involving coordinated and non-coordinated water molecules, leading to a supramolecular arrangement of six chains around a 3-fold inversion axis, with channels running through the crystals along the *c*-axis direction. The O4 atoms belonging to noncoordinated water molecules lie in channels at the 3-fold axis and are involved in hydrogen-bond interactions with the sulfur atoms (S···O4 = 3.331(2) Å). Since neighboring chains are related by centers of symmetry, they exhibit opposite helicity, and therefore the whole structure is not chiral.

The strong coordination of the thiocyanate ligand to the copper(II) ion (Cu−N = 1.914(4) Å) leads to the zigzag helical chain structure instead of the linear chain structure observed for **2** and **3**.

The crystal structure of [Cu(μ-pymca)N_3], **5**, is made of zigzag pymca-bridged copper(II) chains connected by double end-on azide bridging ligands to afford a distorted (6,3) honeycomb network in the *ab* plane (Figure 5).

There are two crystallographically independent copper(II) ions in the structure, namely, Cu and Cu1, which exhibit distorted octahedral CuN_4O_2 chromophores. In the Cu coordination environment, two pyrimidyl and two azide nitrogen atoms are located in equatorial positions, whereas the carboxylate oxygen atoms from the pymca ligands are coordinated in axial positions at a longer distance. Cu1 is also coordinated to two pyrimidyl and two azide nitrogen atoms and to two carboxylate oxygen atoms from the pymca ligands. In this case, however, the cis Cu−N_{azide} bond distances of 2.222(3) Å are the longest ones, and the Cu−O bonds are located in the cis position. It should be noted that, on one side of the honeycomb layer, and within each hexagonal ring, the pyrimidine rings of the ligands are

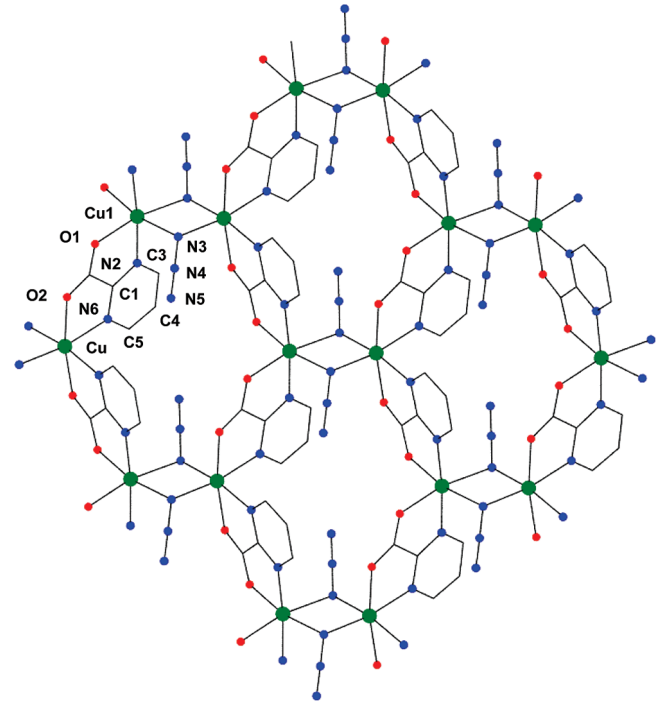

Figure 5. The (6,3) honeycomb layer structure of **5** in the *ab* plane.

alternatively tilted (~56°) toward and away from the normal to the ring. Consequently, on the other side of the layer, carboxylate groups follow the opposite sequence. The dihedral angle between the planes of neighboring ligands is 83.68(2)°, whereas the dihedral angle between the mean planes of the ligand and the Cu(N_3)$_2$Cu dinuclear fragment is 86.75(2)°. The end-on azide bridging ligands are tilted 48.5(2)° with respect to the mean plane of the Cu(N_3)$_2$Cu dinuclear fragment. Neighboring sheets, which are related

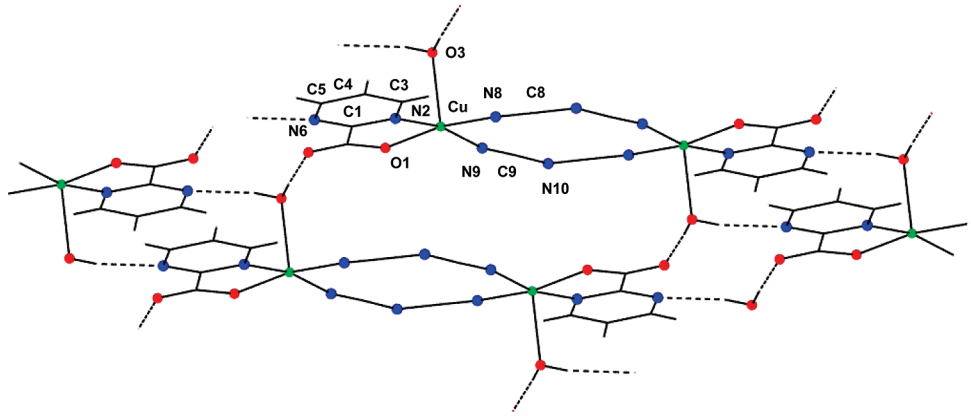

Figure 6. Perspective view of the crystal structure of **6**.

by centers of symmetry, present $\pi-\pi$ stacking interactions with a separation between mean planes of the phenyl rings of 3.528(2)° (see Figure S2, Supporting Information). These interactions lead to an ABAB... repeating pattern of the layers along the *c* direction.

Although several examples of honeycomb layered compounds with alternating bis(chelating) 2,2′-bipyrimidine and double end-on azide bridging ligands have been reported so far, none of them contains copper(II) ions.[15] Moreover, as far as we know, this is the first report concerning a honeycomb structure in which two bis(chelating) bridges alternate with one double end-on azide bridge within the hexagonal rings. Such a unique structure may be a consequence of the different charge balance requirements for pymca and 2,2′-bipyrimidine ligands.

The crystal structure of **6** is made of centrosymmetric dinuclear units [Cu(pymca)(μ-dca)$_2$Cu(pymca)] connected through hydrogen bonds to form a 2D network in the *bc* plane (Figure 6).

Within the dinuclear unit, copper(II) atoms are bridged by two dca anions in an end-to-end fashion. Each copper atom exhibits a square-pyramidal CuN_3O_2 chromophore (Addison's parameter $\tau = 0$).[16] The basal plane is formed by two nitrogen atoms of the dca bridging ligands and one oxygen atom and one nitrogen atom belonging to the bidentate pymca ligand with bond distances of about 2 Å. These four atoms are nearly coplanar, with a deviation of the copper atom from the mean plane of 0.15 Å. The apical position is occupied by a water molecule at a longer distance (2.222(2) Å). The Cu···Cu distance through the dca-bridging group is 7.114 Å. The dinuclear molecules are connected by two couples of complementary hydrogen bonds involving the water molecule and the O2 and N6 atoms belonging to the pymca ligand with donor−aceptor distances of 2.932(2) Å (N6···O3) and 2.731(2) Å (O2···O3). These hydrogen-bond interactions lead to the formation of planar sheets, the shortest Cu···Cu interlayer distance being 5.139 Å.

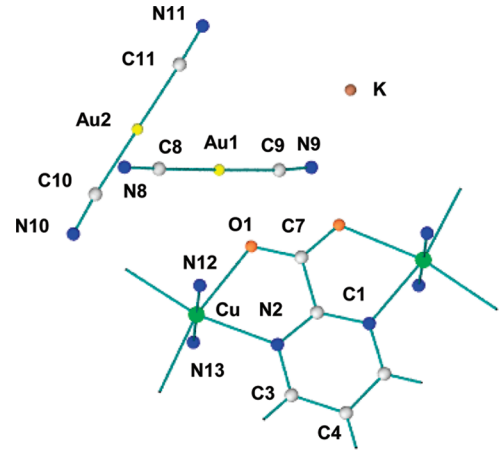

Figure 7. Asymmetric unit of **7**.

The structure of K{[μ-Au(CN)$_2$]$_2$[(Cu(NH$_3$)$_2$)$_2$(μ-pymca)]}-[Au(CN)$_2$]$_2$, **7**, is very similar to that previously reported by us for {[μ-Au(CN)$_2$]$_2$[(Cu(NH$_3$)$_2$)$_2$(μ-bpm)]}[Au(CN)$_2$]$_2$[16] and consists of [Cu(NH$_3$)$_2$(μ-pymca)Cu(NH$_3$)$_2$] dinuclear units connected to four other dinuclear units by [Au(CN)$_2$]$^-$ anions, giving rise to a cationic 2D (4,4) rectangular-grid network. The charge of the structure is balanced by two noncoordinated [Au(CN)$_2$]$^-$ anions and one K cation (Figure 7).

Within the dinuclear fragment, the Cu^{II} ions exhibit a CuN_5O distorted octahedral coordination environment. In this description, one nitrogen and one oxygen atom belonging to a pymca ligand and two nitrogen atoms belonging to two different [Au(CN)$_2$]$^-$ anions are coordinated to the Cu^{II} ions in the plane of the pymca bridging ligand, whereas, below and above this plane, two NH_3 molecules are coordinated.

The Cu−N distances are similar to those observed in {[μ-Au(CN)$_2$]$_2$[(Cu(NH$_3$)$_2$)$_2$(μ-bpm)]}[Au(CN)$_2$]$_2$, the distortion of the CuN_5O coordination polyhedron being through a compression, where the axial distances Cu−NH_3 are considerably shortened with respect to those in the equatorial plane. Since NH_3 is a much stronger σ donor than pymca, the ligand field asymmetry is dominant, leading to an unusual tetragonally compressed geometry.

Within the planar rectangular-grid layer, two of the corners are occupied by two Cu^{II} ions, whereas the other two are found at the pymca ligands (Figure 8). The Cu···Cu distance

(15) (a) De Munno, G.; Poerio, T.; Viau, G.; Julve, M.; Lloret, F.; Journaux, Y.; Riveiere, E. *Chem. Commun.* **1996**, 2587. (b) De Munno, G.; Julve, M.; Viau, G.; Lloret, F.; Faus, J.; Viterbo, D. *Angew. Chem., Int. Ed.* **1996**, *35*, 1807. (c) Cortes, R.; Lezama, L.; Pizarro, J. L.; Arriortua, M. I.; Rojo, T. *Angew. Chem., Int. Ed.* **1996**, *35*, 1810.

(16) Addison, A. W.; Rao, T. N.; Reedijk, J.; van Rijn, J.; Verschoor, G. C. *J. Chem. Soc., Dalton Trans.* **1984**, 1349.

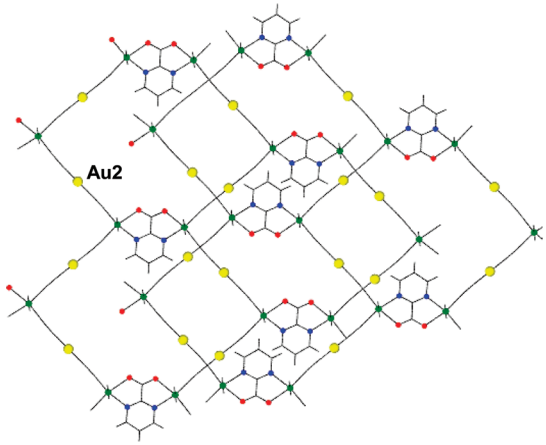

Figure 8. Planar rectangular grid layers of **7**. The noncoordinated dicyanoaurate anions are omitted for clarity.

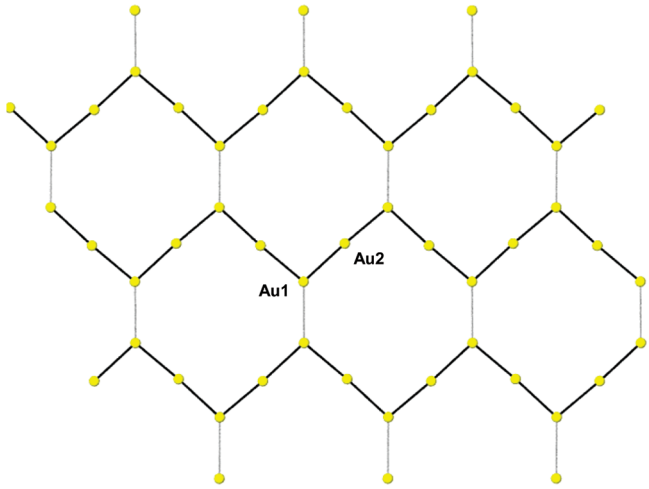

Figure 9. Honeycomb 2D network of gold atoms formed by aurophilic interactions.

across the pymca ligand is 5.786(2) Å, whereas the M···Au distances across the cyanide ligand are 5.192(2) and 5.298(2) Å. Layers are stacked in such a way that the ammonia-coordinated molecules are interdigitated and aligned above and below each sheet with cavities in neighboring sheets, giving rise to an ABAB... repeating pattern of layers, the interlayer distance being 3.69 Å. This relatively short interlayer separation is clearly due to the presence of aurophilic interactions.

Dicyanoaurate anions and K cations, which play a filling space and charge compensating role in the structure, are located between layers. Gold atoms of bridging and non-bridging dicyanoaurate anions are involved in short aurophilic interactions (Au1−Au2 distances are in the range 3.15−3.16 Å), leading to a chain of gold atoms running along the *c* direction (Figure 9) with a Au2−Au1−Au2 angle of 97.54(3)°. The Au−Au distances are among the shortest observed for $[Au(CN)_2]^-$ anions involved in aurophilic interactions.[17−19]

Theoretical studies and experimental results have shown that the Au···Au distances decrease with an increase in the torsion angle between adjacent $[Au(CN)_2]^-$ units.[18c,19] In keeping with this and with the short Au−Au distances observed for **7**, adjacent $[Au(CN)_2]^-$ anions are staggered with a C−Au1−Au2−C torsion angle of 57.5°. Neighboring chains are further connected by weaker aurophilic interactions with Au1−Au1 distances of 3.447 Å, affording a honeycomb-like 2D network of gold atoms with interlayer distances of 9.65 Å. The (4,4) rectangular sheets and (6,3) honeycomb sheets share the Au2 atoms and make dihedral angles of 51.61°, leading to a unique 3D network (Figure 9). K cations, which are disordered on two positions, are located between layers near the carboxylate part of the pymca ligands, with K−O distances of 2.560(1) Å.

Magnetic Properties. The temperature dependences of χ_M and $\chi_M T$ for **1** (χ_M is the molar magnetic susceptibility per Cu(II) ion) in an applied magnetic field of 0.5 T are displayed in Figure S3 (Supporting Information). At room temperature, the $\chi_M T$ product (0.435 $cm^3\ mol^{-1}$ K) matches well with the spin-only value expected for one Cu(II) ion with $S = 1/2$ and $g = 2.15$ and remains almost constant down to about 25 K. Below this temperature, the $\chi_M T$ product decreases to 0.346 $cm^3\ mol^{-1}$ K at 2 K. This behavior is indicative of the presence of a weak antiferromagnetic interaction between the Cu(II) ions through the pymca bridging ligand. Since **1** is a linear chain complex, the susceptibility data were fitted using the equation derived from the Bonner−Fischer calculation for an antiferromagnetic chain of equally spaced copper(II) ions, on the basis of the isotropic Hamiltonian $H = -J \sum_i (S_i\ S_{i+1})$.[20] The best fit parameters were $J = -0.57(1)\ cm^{-1}$ and $g = 2.16(1)$. The low value of the exchange coupling constant, *J*, can be related to the nature of the bridge between neighboring copper(II) ions. The magnetic coupling in this compound takes place through the carboxylate group of the ligand in a *syn*−*anti* conformation, which links basal (short) and axial (long) positions on the neighboring copper(II) ions. This exchange pathway produces always very small coupling (either antiferro- or ferromagnetic) regardless of the structural parameters of the bridge.[21] This is because (i) the axial Cu−O_2 distance is long and (ii) the magnetic orbital on the Cu(II) is mainly located in the equatorial plane, and therefore the spin density on its axial position is expected to be very small. Nevertheless, the fact that the O−Cu−O axis of the CuN_2O_4 distorted octahedral coordination polyhedron is tilted away from the normal to

(17) Suárez-Varela, J.; Sakiyama, H.; Cano, J.; Colacio, E. *Dalton Trans.* **2007**, 249.

(18) (a) Leznoff, D. B.; Lefebvre, J. *Gold Bull.* **2005**, *38*, 47, and references therein. (b) Zhou, H.-B.; Wang, S.-P.; Dong, W.; Liu, Z.-Q.; Wang, Q.-L.; Liao, D.-Z.; Jiang, Z.-H.; Yan, S.-P.; Cheng, P. *Inorg. Chem.* **2004**, *43*, 4552. (c) Assefa, Z.; Omary, M. A.; McBurnett, B. G.; Mohamed, A. A.; Patterson, H. H.; Staples, R. J., Jr. *Inorg. Chem.* **2002**, *41*, 6274. (d) Colacio, E.; Lloret, F.; Kivekäs, R.; Suárez-Varela, J.; Sundberg, M. R.; Uggla, R. *Inorg. Chem.* **2003**, *42*, 560. (e) Lefebvre, J.; Callaghan, F.; Katz, M. J.; Sonier, J. E.; Leznoff, D. B. *Chem.—Eur. J.* **2006**, *12*, 6248. (f) Lefebvre, J.; Chartrand, D.; Leznoff, D. B. *Polyhedron* **2007**, *26*, 2189. (g) Katz, M. J.; Kaluarachchi, H.; Batchelor, R. J.; Bokov, A. A.; Ye, Z.-G.; Leznoff, D. B. *Angew. Chem., Int. Ed.* **2007**, *46*, 8804.

(19) Colacio, E.; Lloret, F.; Kivekäs, R.; Suárez-Varela, J.; Sundberg, M. R. *Chem. Commum.* **2002**, 592.

(20) Bonner, J. C.; Fischer, M. E. *Phys. Rev. A: At., Mol., Opt. Phys.* **1964**, *135*, 640.

(21) (a) Colacio, E.; Ghazi, M.; Kivekäs, R.; Moreno, J. M. *Inorg. Chem.* **2000**, *39*, 2882. (b) Baldomá, R.; Monfort, M.; Ribas, J.; Solans, X.; Maestro, M. *Inorg. Chem.* **2006**, *45*, 8144.

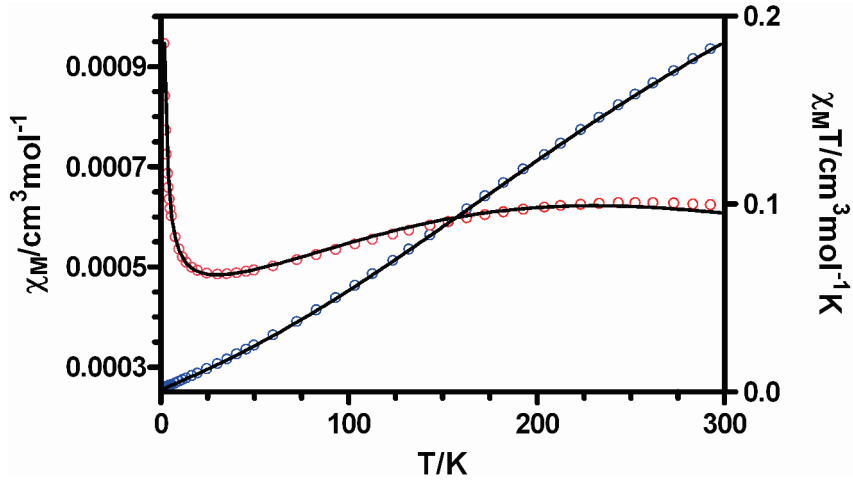

Figure 10. Plots of χ_M (left) and $\chi_M T$ (right) for **2**. The solid line corresponds to the best fit.

the equatorial plane could lead to a non-negligible spin density on the axial positions and, consequently, favor a weak antiferromagnetic interaction.

The temperature dependences of χ_M and $\chi_M T$ for **2** (χ_M is the molar magnetic susceptibility per Cu(II) ion) in an applied field of 0.5 T are given in Figure 10.

The value of the $\chi_M T$ product at room temperature (0.186 $cm^3\ mol^{-1}\ K$) is significantly lower than that expected for an uncoupled Cu(II) ion with $g = 2$ (0.375 $cm^3\ mol^{-1}\ K$), which is probably due to the existence of medium to strong antiferromagnetic interactions between the copper(II) ions mediated by the bisbidentate pymca bridging ligand. The $\chi_M T$ product shows a continuous decrease with decreasing temperature to reach a value of 0.0019 $cm^3\ mol^{-1}\ K$ at 2 K, thus supporting the presence of antiferromagnetic interactions between Cu(II) ions. In keeping with this, the thermal variation of χ_M shows a maximum near 252 K. Below this temperature, χ_M decreases to reach a minimum at 20 K and then increases to a value of 0.0009 $cm^3\ mol^{-1}\ K$ at 2 K. This low-temperature tail is due to the presence of a small amount of mononuclear impurity. As indicated elsewhere, complex **2** can be viewed as formed by cationic chains of trans-pymca-bridged copper(II) ions connected by bromide anions. The interaction through the bromide bridging ligand is expected to be very small (almost negligible), owing to the long Cu−Br bond distances and the coordination of the bromide ligand in axial position where the spin density of the unpaired electron is, if at all, very small (the dx^2-y^2 magnetic orbital is directed to the equatorial nitrogen and oxygen atoms of the trans-coordinated pymca ligands). As a result, only the J parameter through the bisbidentate pymca bridges needs to be considered. Taking this into account, the magnetic data were fitted to the equation for an antiferromagnetic chain of equally spaced copper(II) ions,[20] in which a P parameter was included to account for the mononuclear impurity. The best fit parameters were $J = -276.1(1)\ cm^{-1}$, $g = 2.122(1)$, and $P = 0.002$. The strong antiferromagnetic interaction occurring in **2** can be ascribed to the fact that the magnetic orbitals centered on nearest neighbor copper ions are located in the plane of the pymca bridging ligand, and therefore, they are favorably oriented

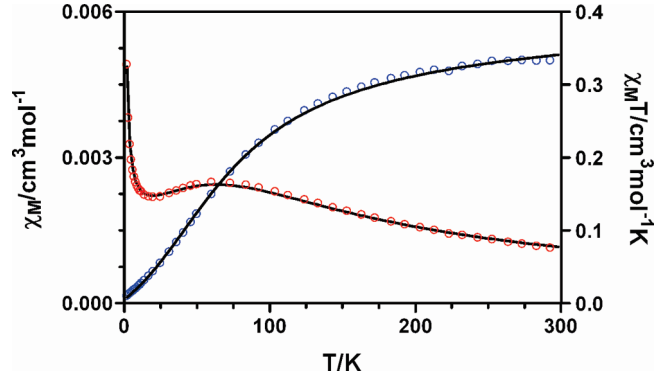

Figure 11. Temperature dependence of χ_M (left) and $\chi_M T$ (right) for **3**. The solid line is a fit to the experimental data using the values given in the text.

to overlap on both sides of the pymca group. Recently, we have shown through theoretical calculations and experimental results that the pymca ligand is able to produce medium to strong antiferromagnetic interactions that are intermediate between those produced by oxalate and 2,2′-bipyrimidine.[3] Polynuclear copper(II) complexes with bisbidentate oxalato bridging ligands that connect equatorial positions on planar, square-based pyramidal or 4 + 2 tetragonally elongated distorted octahedral copper(II) ions exhibit $-J$ values in the range 290−400 cm^{-1},[22] whereas the analogous bipyrimidine-bridged complexes show $-J$ values in the range 139−238 cm^{-1}.[23] The J value for **2** of $-276.1\ cm^{-1}$ is, as expected, intermediate between the above indicated values for the oxalate and bipyrimidine-bridged dinuclear planar copper(II) complexes.

The magnetic properties of complex **3** are shown in Figure 11 in the form of χ_M and $\chi_M T$ versus T.

The room temperature $\chi_M T$ value (0.333 $cm^3\ mol^{-1}\ K$) is slightly lower than that expected for magnetically isolated copper(II) ions, thus suggesting the existence of an antiferromagnetic interaction between copper(II) ions. Upon cooling from room temperature, the $\chi_M T$ product steadily decreases

(22) Julve, M.; Verdaguer, M.; Gleizes, A.; Philoche-Levisalles, M.; Khan, O. *Inorg. Chem.* **1984**, *23*, 3808.
(23) De Munno, G.; Julve, M.; Lloret, F.; Cano, J.; Caneschi, A. *Inorg. Chem.* **1995**, *34*, 2048.

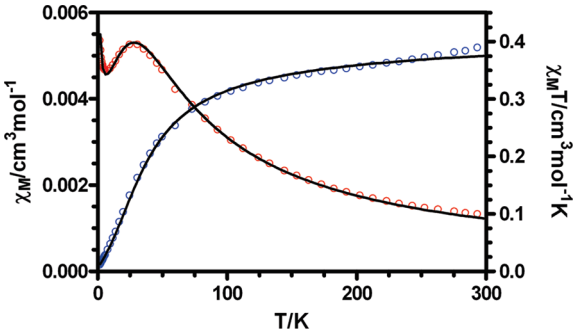

Figure 12. Experimental temperature dependence of χ_M (left) and $\chi_M T$ (right) for **4**. The solid line represents the best fitting.

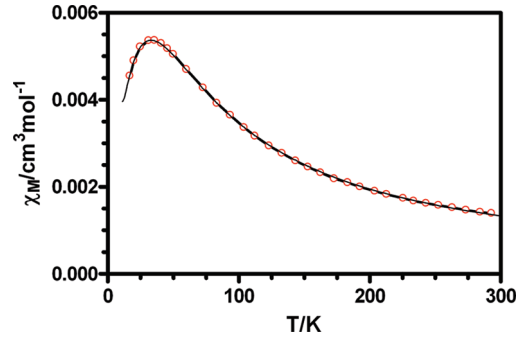

Figure 13. Thermal dependence of χ_M (per copper ion) in **5**. The circles and lines represent, respectively, the experimental data and the simulation using the parameters obtained in the fit process.

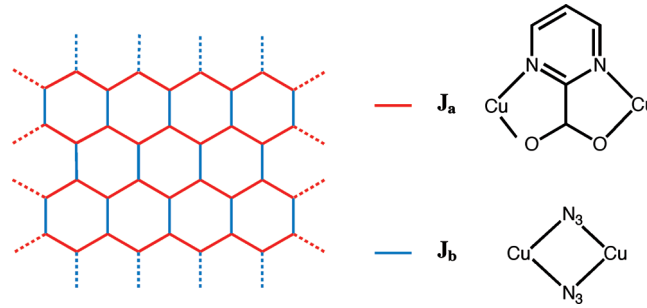

Figure 14. Topology interaction observed in **5** matching with an alternating 2D honeycomb.

and reaches a value of 0.01 $cm^3\ mol^{-1}$ K. The temperature dependence of χ_M shows a maximum near 65 K, thus confirming the existence of a weak to medium antiferromagnetic interaction between the copper(II) ions, which is mainly mediated by the pymca-bridged ligands. The best fit of the susceptibility data to the equation for an antiferromagnetic chain of equally spaced copper(II) ions,[20] with the inclusion of a P parameter to account for the mononuclear impurity, leads to the following magnetic parameters: $J = -72.5(5)\ cm^{-1}$, $g = 2.125$, and $P = 0.015$. In spite of the structural similarity between **2** and **3** (4 + 2 elongated octahedral copper coordination environment and planar Cu−pymca−Cu−pymca fragment), the J value for the latter is significantly lower than for the former. In order to try to justify the low J value observed for **3**, we have performed DFT theoretical calculations (see below in the DFT calculations section).

The temperature dependences of χ_M and $\chi_M T$ (χ_M being the magnetic susceptibility per copper atom) for **4** are shown in Figure 12.

The value of $\chi_M T$ at room temperature (0.384 $cm^3 mol^{-1} K$) is characteristic of a magnetically isolated spin doublet. The appearance of a maximum in the χ_M versus T plot near 28 K and the decreasing of $\chi_M T$ upon cooling suggest dominant antiferromagnetic interactions. In keeping with the uniform chain structure of **4**, the susceptibility data were fitted to the equation for an antiferromagnetic chain of equally spaced copper(II) ions,[20] leading to $J = -31.4(2)\ cm^{-1}$, $g = 2.070(6)$, and $P = 0.01$. As indicated above, the coordination environment of the copper(II) ion in **4** adopts an elongated rhombic geometry with three short Cu−N, one short Cu−O, and two long Cu−O distances. The magnetic orbital, which points toward the four nearest neighbors of the copper atom, is alternatively located along the chain in the plane of the pymca bridging ligand for a copper atom and in the plane perpendicular to the pymca ligand for the neighbor copper atom. Now, only the Cu−pyrimidine−Cu pathway is operative, and therefore the interaction along the chain decreases significantly with regard to those observed for **2** and **3**, where both the pyrimidine and carboxylato pathways were operative.

The $\chi_M T$ values for **5** do not show significant change (about 0.38 $cm^3\ mol^{-1}$ K) above 150 K. Below this temperature, however, $\chi_M T$ gradually decreases down to 2 K, whereas the χ_M versus T plot exhibits a maximum near 35 K (Figure 13).

As indicated elsewhere, compound **5** exhibits a honeycomb layer structure, in which two pymca bridges alternate with one double end-on azide bridge within the hexagonal rings (Figure 14). Because an analytical law is not known for this complicated network topology with local quantum $S = 1/2$ spin moments, we have used quantum Monte Carlo (QMC) methods to interpret the experimental magnetic data. The QMC method used for this purpose was that called the decoupled cell method, proposed by Homma et al., where the full system is split into several subsystems (cells) that have a size small enough to obtain the probability of each configuration by diagonalization of the energy matrix.[24,25] These probabilities are used to calculate the spin flip probabilities, that is, the probability to reverse a local spin moment in a certain spin configuration of the full system. Thus, the applicability of this method will be restricted to the temperature region where the spin correlation length is shorter than the used cell. As a consequence, using larger subsystems allow us to correctly apply this method at lower temperatures.

In the MC methods, from the spin flip probabilities and using a metropolis algorithm, we can generate a sampling where the states more present are those having a more important contribution in the partition function. This sampling allows us to calculate the average magnetization at a

(24) Homma, S.; Sano, K.; Matsuda, H.; Ogita, N. *Prog. Theor. Phys. Suppl.* **1986**, 127.
(25) Homma, S.; Matsuda, H.; Ogita, N. *Prog. Theor. Phys. Suppl.* **1986**, *75*, 1058.

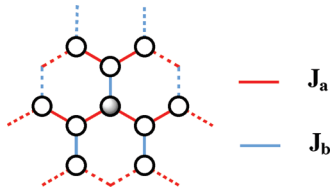

Figure 15. Decomposition in small cells of a honeycomb network which are used in the MC simulations. Broken lines refer to the global exchange topology, whereas the bold ones represent the cell obtained in the decomposition process. While the darkened circle is the central site in a given cell, the white circles are the remaining sites in the same cell.

given temperature. The molar magnetic susceptibility can be obtained from the fluctuations in the magnetization through eq 1, where $\langle M\rangle$ and $\langle M\rangle^2$ are the mean values of the magnetization and its square, and N, β, and k have their usual meaning.

$$\chi_M T = N\beta^2/k(\langle M^2\rangle - \langle M\rangle^2) \quad (1)$$

In all simulations, the number of MC steps for each temperature is $5 \times 10^6/T$ (T in K). Thus, we included more steps in the sampling at low temperatures where the correct equilibrium requires more recorded data. A total of 10% of the MC steps are employed for the thermalization of the system; thus, we stocked the physical properties when the equilibrium was reached. A model of 30×30 sites was used in the simulations. Periodic boundary conditions were introduced in all simulations. Deeper details on the MC simulations can be found in ref 26.

In our simulations, we have broken down the network in small cells that include the central site that undergoes a spin-flip and the first and second neighbors (see Figure 15). Several $\chi_M T$ versus $T/|J_i|$ simulations have been done for different values of the ratio $|J_j|/|J_i|$ (α), where α takes values that are comprised between 0 and 1. Thus, in all cases, the value of $|J_i|$ is larger than that presented by $|J_j|$. Because in our spin network there are two exchange couplings, one ferromagnetic and one antiferromagnetic, two sets of simulations have been done, one of them being the strongest in each set. Analytical laws for each case have been extrapolated by fitting the data obtained from the Monte Carlo simulations to a quotient between two polynomial functions that depends on the temperature, allowing us to fix a constant value at higher temperatures that corresponds with that expected for an isolated copper(II) ion. These laws take the form of eq 2. The values of its coefficients are shown in Tables 2 and 3 for an $S = 1/2$ alternating honeycomb network with a ferro- and an antiferromagnetic coupling as the predominant interaction, respectively.

$$\chi_M T = \frac{g_{Cu}^2}{4} \frac{\sum_{i=0}^{4}\sum_{j=0}^{1} a_{i,j}\cdot\beta^i\cdot\alpha^j}{\sum_{i=0}^{4}\sum_{j=0}^{1} b_{i,j}\cdot\beta^i\cdot\alpha^j} \quad (2)$$

Two conclusions were reached when both expressions were used to reproduce the experimental data: (i) it was necessary to include a paramagnetic impurity, which was removed in the final data, and (ii) a predominant ferromagnetic interaction is suggested in both cases. In spite of the fact that the weakest coupling is antiferromagnetic, its effect is prevailing in the $\chi_M T$ versus T curve due to a larger presence of it. The least-squares fits of the experimental data give exchange coupling constant values of $+71 \pm 11$ and -34 ± 7 cm^{-1} for J_a and J_b, respectively. The g-factor value found for the copper(II) ions in **5** is 2.038 ± 0.009. The agreement factor, defined as $F = \sum[(\chi_M T)_{exp} - (\chi_M T)_{calcd}]^2/\sum[(\chi_M T)_{exp}]^2$, is 2×10^{-5}. These values for the exchange coupling constants are weaker than those expected from the experimental data in this and previous works.[3,27] A detailed analysis of these results has been done from DFT calculations (see below).

The magnetic properties of complex **6** in the form of χ_M and $\chi_M T$ versus T (χ_M being the molar susceptibility per dinuclear unit) are shown in Figure 16.

Table 2. Coefficients in the Empirical Law That Connect the $\chi_M T$ Product with the Exchange Coupling Constants (J_a and J_b) and the Temperature for an $S = 1/2$ Ferro−Antiferro Alternating Honeycomb Network with a Predominant Ferromagnetic Coupling[a]

i	j	$\alpha_{i,j}$	$\beta_{i,j}$	i	j	$\alpha_{i,j}$	$\beta_{i,j}$
0	0	0	0.0302978	2	2	168.706	177.991
0	1	0	1.0966	3	0	645.985	979.162
1	0	0.389577	−0.333124	3	1	−893.562	−1168.74
1	1	2.89813	−73.0225	3	2	−105.264	315.186
2	0	−31.6167	−24.5132	4	0	998.9025	2663.74
2	1	−95.0719	996.144	4	1	484.125	1291.0

[a] This law is expressed as in eq 2. The parameters β and α are defined as $T/|J_b|$ and $|J_a|/|J_b|$, respectively. The coefficients that have been considered zero do not appear in the table.

Table 3. Coefficients in the Empirical Law That Connect the $\chi_M T$ Product with the Exchange Coupling Constants (J_a and J_b) and the Temperature for an $S = 1/2$ Ferro−Antiferro Alternating Honeycomb Network with a Predominant Antiferromagnetic Coupling[a]

i	j	$\alpha_{i,j}$	$\beta_{i,j}$	i	j	$\alpha_{i,j}$	$\beta_{i,j}$
0	0	0	0.403422	2	1	−0.123109	−0.926531
0	1	0	−0.0362409	3	0	2.73691	8.66979
1	0	0.0154042	0.931194	3	1	1.21881	2.52666
1	1	0.149732	2.24815	4	0	1.0447875	2.7861
2	0	−0.484058	3.30334	4	1	−0.072878625	−0.194343

[a] This law is expressed as in eq 2. The parameters β and α are defined as $T/|J_a|$ and $|J_b|/|J_a|$, respectively. The coefficients that have been considered zero do not appear in the table.

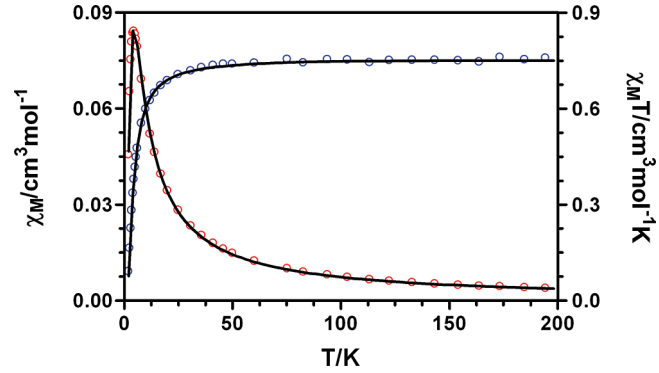

Figure 16. Temperature dependence of χ_M (left) and $\chi_M T$ (right) for **6**. The solid line is a fit to the experimental data using the values given in the text.

(26) Cano, J.; Journaux, J. In *Magnetism: Molecules to Materials*; Miller, J. S., Drillon, M., Eds.; VCH: Weinheim, Germany, 2005.
(27) Ruiz, E.; Cano, J.; Alvarez, S.; Alemany, P. *J. Am. Chem. Soc.* **1998**, *120*, 11122.

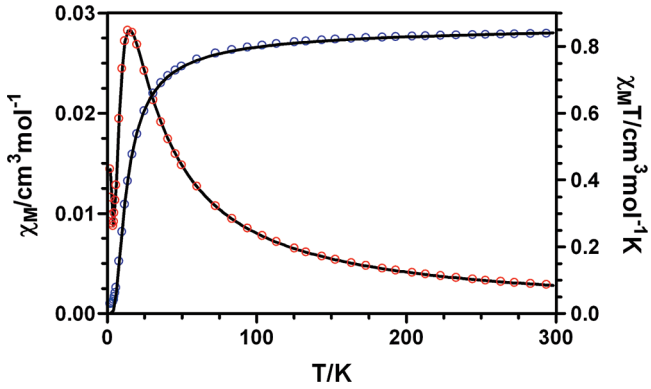

Figure 17. Plots of χ_M (left) and $\chi_M T$ (right) for **7**. The solid line corresponds to the best fit.

In this case, the appearance of a maximum near 5 K and the sudden decrease of the $\chi_M T$ value below 40 K indicate the existence of a very weak antiferromagnetic coupling between copper centers through the dicyanamide bridges. As **6** is a dinuclear complex, the susceptibility data were analyzed using the Bleaney−Bowers expression for two magnetically interacting spin doublets derived from the isotropic Hamiltonian, $H = -JS_1S_2 + g\beta(S_1S_2)$, with the inclusion of a P parameter to account for the presence of paramagnetic impurity. Least-squares best-fit results were $J = -5.1(1)$ cm^{-1}, $g = 2.00(4)$, and $P = 0.03(1)$. The J value for **6** is similar but slightly higher than those found for other μ-1,5-dicyanamide-bridged dinuclear complexes with dicyanamide ligands linking two equatorial positions on neighboring copper atoms, which are found between −3.3 and −4.4 cm^{-1}.[28] This fact may be due to an overestimation of the antiferromagnetic interaction, as the interactions through the hydrogen bond pathways were not taken into account. Anyway, the results confirm that the μ-1,5-dicyanamide bridge is a very poor mediator of the magnetic exchange interaction.

The temperature dependences of χ_M and $\chi_M T$ (χ_M is the molar magnetic susceptibility per dinuclear unit) in an applied magnetic field of 0.5 T for **7** are shown in Figure 17.

The room-temperature $\chi_M T$ value of 0.834 cm^3 mol^{-1} K for **7** agrees well with that expected for two isolated Cu(II) ($S = 1/2$) ions. The χ_M curve increases as the temperature is lowered until a maximum is reached at 14 K and then decrease very sharply. At very low temperatures (<10 K), the χ_M curves increase due to the presence of a small amount of paramagnetic impurity. The occurrence of this maximum in χ_M is indicative of the existence of an antiferromagnetic coupling between the metal ions. In keeping with this, the $\chi_M T$ curve exhibits a continuous decrease upon cooling down to a value very close to zero. Because the magnetic exchange interaction through the dicyanoaurate bridging groups, if any exists, is negligible, compound **7** could be considered from the magnetic point of view as a dinuclear system. The magnetic data were fitted to the Bleaney−Bowers expression derived from the isotropic Hamiltonian: $H = -JS_1S_2 + g\beta(S_1S_2)$. A term accounting for the paramagnetic impurity was included in the equation. The best fit parameters were $J = -17.50(1)$, $g = 2.147(1)$, and $P = 0.04(2)$. The relatively low J value for **7** can be explained by the unusual axial compressed geometry of the copper(II) ion. In a simple way, we can predict that an axial compression causes a decrease and an increase of the energies of x^2-y^2 and z^2 orbitals, respectively, which could lead to a change in the nature of the magnetic. Since only two-thirds of the electronic density of the z^2 orbital is placed in the equatorial plane and not placed only in the direction of the metal−ligand bond, there is a decrease in the overlapping between this orbital and the ligand orbitals, similar to a case where the x^2-y^2 is the magnetic orbital. As a consequence, a weakening of the antiferromagnetic exchange coupling is expected. Recently, theoretical calculations and experimental results have confirmed this prediction in the analogous bipyrimidine-bridged compound $\{[\mu\text{-Au(CN)}_2]_2[(\text{Cu(NH}_3)_2)_2(\mu\text{-bpm})]\}[\text{Au(CN)}_2]_2$.[17] Although pymca is a better mediator of the magnetic exchange interaction than bpm, the exchange coupling constant for this latter compound ($J = -20$ cm^{-1}) is higher than that observed for **7**. This fact might be due to small structural differences affecting bond distances and angles in the copper coordination polyhedra. A summary of the magnetic properties of the seven compounds is gathered in Table 4.

DFT Calculations. In order to explain the unexpected magnitudes of the magnetic exchange couplings in some of the compounds presented in this paper (**3** and **5**), we have carried out a theoretical study based on density functional theory. The first question to answer deals with the very different strength of the magnetic exchange coupling between copper(II) ions in **2** and **3**. From a chemical point of view, these compounds are very similar, displaying an axial Jahn−Teller effect that places the equatorial plane of the metal ion in the same plane of the pymca ligand, thus favoring a one-dimensional arrangement and a large overlapping between the copper(II) magnetic orbitals. Therefore, as indicated elsewhere, a strong antiferromagnetic coupling is expected for both compounds, which must be intermediate between those observed for oxalate and 2,2′-bipyrimidine-bridged copper(II) complexes, which (as in **2** and **3**) connect equatorial positions on the coordination sphere of the copper(II) ions.[22,23] In principle, the fact that the J value for **3** is significantly lower than that for **2** might be only due to the main differences observed between both structures, which, as indicated elsewhere, are as follows: (i) the axial positions of the metal ion are occupied by different halides (X = Br$^-$ or Cl$^-$) in **2** and **3**. Since Cu−X distances are very long, the Cu−X−Cu pathway must not have an important influence on the magnetic exchange coupling, and (ii) there are different dispositions of the pymca ligands around the copper(II) ion along the chain (cis in **2** and trans in **3**).

To carry out this study, we have built two dinuclear model complexes from the experimental crystal structures (see outlined models in Figure 18). In both cases, to avoid highly negatively charged complexes, square-planar copper(II) ions have been considered by removing the halides located on

(28) Van Albada, G. A.; van der Horst, M. G.; Mutikainen, I.; Turpeinen, U.; Reedijk, J. *Inorg. Chem. Comum.* **2007**, *10*, 1014.

Table 4. Summary of Magnetic Properties for Compounds **1**−**7**

compound	-J/cm^{-1}	ligands bridging mode	magnetic orbitals
1	−0.57(1)	*syn*−*anti*-carboxylate pymca O-equatorial/O-axial	dx^2-y^2/dx^2-y^2
2	−276.1(1)	*cis*-bis(chelating) pymca (N,O-equatorial)/(N,O-equatorial)	dx^2-y^2/dx^2-y^2
3	−72.5(5)	*trans*-bis(chelating) pymca (N,O-equatorial)/(N,O-equatorial)	dx^2-y^2/dx^2-y^2
4	−31.4(2)	bis(chelating) pymca (N,O-equatorial.)/(N-equatorial-O-axial)	dx^2-y^2/dx^2-y^2
	−34(7)(pymca)	bis(chelating) pymca (N-equatorial-O-axial)/(O-equatorial-N-axial)	dx^2-y^2/dz^2
5	71(11)(azide)	double *end-on* azide N-equatorial./N-equatorial	dx^2-y^2/dz^2
6	−5.1(1)	double 1,5-dicyanamide N-equatorial/N-equatorial	dx^2-y^2/dx^2-y^2
7	−17.50(1)	bis(chelating) pymca N,O-equatorial/N,O-equatorial	dz^2/dz^2

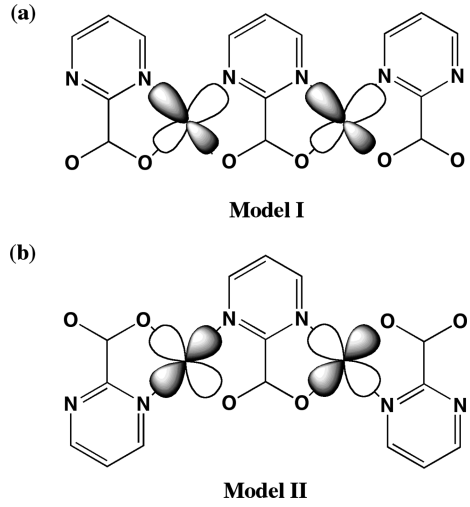

Figure 18. Outlined d−p hybridation of the metal magnetic orbitals in models I and II, which have been built from experimental geometries of **3** and **2**, respectively.

the axial positions. In this situation, it can be presumed that differences in the exchange coupling constants are only due to the different effect of the peripheral ligand;[29] that is, the nitrogen and oxygen donor atoms of the pymca ligand *lead to an unequal hybridation* of the copper dx^2-y^2 magnetic orbital just as it is displayed (assuming a major effect of the oxygen donor atom) in Figure 18. Qualitatively, when the pymca ligands are in a trans arrangement, because the donor atoms in opposite positions are equivalents, the net hybridation is null, and the magnetic orbital of the metal ion can be considered as a pure dx^2-y^2 orbital (Figure 18b). This is not the case in the cis arrangement (Figure 18a). However, since the nitrogen and oxygen atoms of the pyrimidine and carboxylate groups provide similar crystal field ligand strengths, a small difference in the *J* constants for models I and II should be expected, the antiferromagnetic coupling being stronger for model II than for model I. In agreement with this, the values of the exchange coupling constants estimated by means of DFT calculations are −128.3 and −132.0 cm^{-1} for models I and II, respectively. Therefore, an explanation based on changes on the electronic structure is not possible. Despite the absence of any discontinuity in the magnetic data, we think that the only reasonable explanation for the relatively low *J* value observed for **3** would be the existence of a structural change. This geometrical alteration could induce a new spatial disposition of the magnetic orbitals leading to a small overlapping between them. The more convincing geometrical modification would be that in which the Jahn−Teller axis is pointing at the pymca ligand. In this case, a reduction factor for the predominant antiferromagnetic contribution to *J* equal to 1/4 can be envisaged, leading to an exchange coupling constant similar to that extracted from the experimental data (−72.5 cm^{-1}).[20,31] This topology of the magnetic orbitals is also observed in **4**; however, whereas in the proposed case for **3** the Jahn−Teller axis is placed on the less efficient magnetic exchange pathway (oxygen atom), in **4** this axis lies on the more efficient pathway, reducing the magnitude of the magnetic interaction. We are now trying to crystallize the complexes [Cu(pymca)X] (X = NO_3^- and ClO_4^-), which exhibit the same magnetic behavior of complex **3**, but until now, all attempts in this direction were unsuccessful. The structures of these complexes may help us to clarify the origin of the low *J* value observed for **3**.

On the other hand, as observed for **2**, a strong antiferromagnetic exchange coupling ($J_1 = -276.1$ cm^{-1}) is expected for **5** when the pymca acts as a bridging ligand with the magnetic orbitals centered on nearest neighbor copper ions lying in the plane of the pymca bridge. Additionally, two azido groups connect the metal ions from a μ-1,1 coordination (J_2), expanding the interaction topology to a honeycomb network. From a known theoretical magneto-structural correlation published by one of us, a strong ferromagnetic interaction is suspected for J_2 (= +130 cm^{-1}).[32] However, the values of the *J* constants obtained from the experimental data are less than those assumed from the data found in the literature. The understanding of this new discrepancy is the second problem to solve in this section. A detailed analysis

(29) Roman, P.; Guzmán-Miralles, C.; Luque, A.; Beitia, J. I.; Cano, J.; Lloret, F.; Julve, M.; Alvarez, S. *Inorg. Chem.* **1996**, *35*, 3741.
(30) Cano, J.; Alemany, P.; Alvarez, S.; Verdaguer, M.; Ruiz, E. *Chem.*−*Eur.* **1998**, *4*, 476.
(31) Julve, M.; Verdaguer, M.; Gleizes, A.; Philochelevisalles, M.; Kahn, O. *Inorg. Chem.* **1984**, *23*, 3808.
(32) Ruiz, E.; Cano, J.; Alvarez, S.; Alemany, P. *J. Am. Chem. Soc.* **1998**, *120*, 11122.

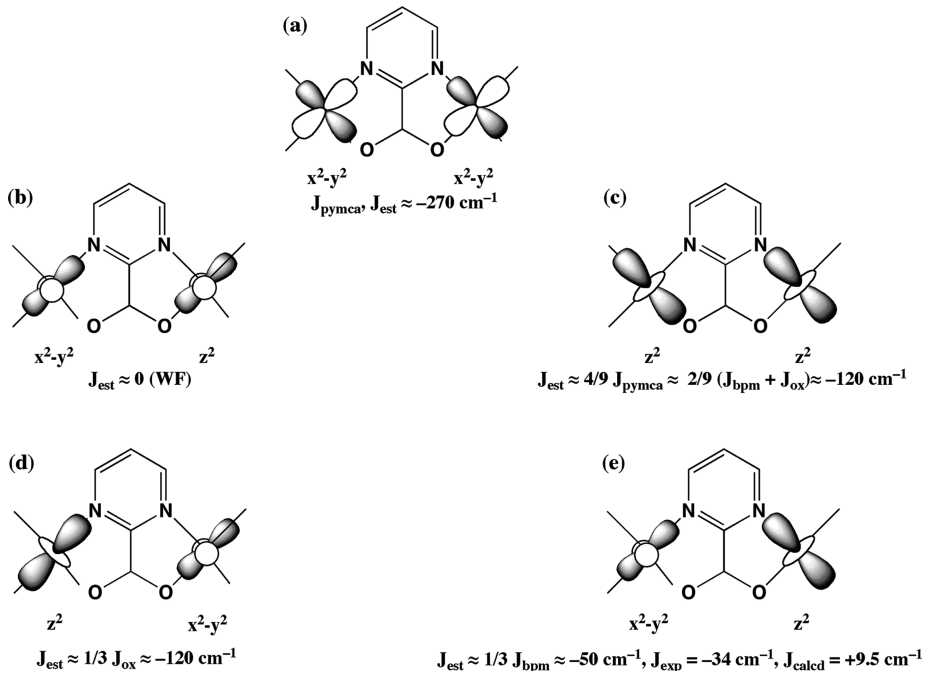

Figure 19. Four possible arrangements (b−e) of the magnetic orbitals in the $[Cu_2(pymca)]$ core of **5**. The usual and ideal arrangement is also displayed (a). The experimental (J_{exp}), estimated (J_{est}), and calculated (J_{calcd}) J constants are given in cm^{-1}. The contractions bpm, ox, and pymca refer to the 2,2′-bipyrimidine, oxalate and, pyrimidine-2-carboxylato ligands, respectively.

of the molecular geometry of the metal coordination sphere in **5** indicates that (i) the metal−ligand distances are longer than those presumed for a 4 + 2 tetragonally elongated distorted octahedral copper(II) ion, (ii) the geometry of the metal sphere coordination cannot be assigned to either a compressed or an elongated octahedral geometry, and (iii) the data seem to suggest an intermediate situation, which could be induced by a dynamic Jahn−Teller effect on the copper(II) ion. This phenomenon, which is rather unusual, has already been observed in some copper(II) complexes where the molecular geometries and electronic structure are strongly dependent on the temperature.[33−40] These static or dynamic situations prevent the discovery of a pure magnetic orbital (usually dx^2-y^2 in copper(II) complexes), leading to a mixture of the two possible magnetic orbitals for axial elongated and compressed geometries, dx^2-y^2 and dz^2, respectively. The degree of combination of these two orbitals to form the magnetic orbital will strongly rely on the geometrical parameters and, therefore, be changeable by the temperature when the effect is dynamic. In a similar copper(II) compound with 2,2′-bipyrimidine and oxalate as bridging ligands organized in a honeycomb network, an intermediate geometry for the coordination sphere of the copper(II) ion was also observed.[41] We think, in these analogues systems, when the one-dimensional system evolves to bidimensional honeycomb network, the axial Jahn−Teller of the metal ion is lost to try a stronger bond with all bridging ligands.

Usually, in real complexes, particularly when different ligands are coordinated to the metal ion, there is no easy way to know this degree of the mixture. That is why DFT calculations can be useful to correctly describe the magnetic properties of these kinds of complexes. In Figures 19 and 20 are shown the four contributions to the exchange coupling when the magnetic orbitals of the copper(II) ions are described as a mixture between the dx^2-y^2 and dz^2 orbitals. The orientation of the orbitals has been taken in the same way that is found in DFT calculations. When the pymca ligand is responsible for transmitting the magnetic coupling, and following the simple ideas set out by Julve et al. in a previous work, we can estimate from the electronic densities of the d orbitals involved in the process a qualitative magnitude for each contribution.[31] Thus, due to a null overlapping between magnetic orbitals in case b, the antiferromagnetic contribution is negligible, and only a weak ferromagnetic coupling is expected. Considering the wave function that describes the different spatial distribution of the electronic densities placed on the axial and equatorial lobes of the dz^2 orbitals, we can assumed that cases d and e are similar and provide an antiferromagnetic contribution that is reduced to 1/3 of the ideal case, where the pymca ligand occupies the equatorial positions of the copper(II) ions and dx^2-y^2 is the magnetic orbital (Figure 19a). The exchange pathways through the pymca ligand can be connected to those present in complexes with oxalate and 2,2′-bipyrimidine

(33) Bacci, M. *New J. Chem.* **1993**, *17*, 67.
(34) Fil, D. V.; Tokar, O. I.; Shelankov, A. L.; Weber, W. *Phys. Rev. B: Condens. Matter. Mater. Phys.* **1992**, *45*, 5633.
(35) Hitchman, M. A.; Maaskant, W.; van der Plas, J.; Simmons, C. J.; Stratemeier, H. *J. Am. Chem. Soc.* **1999**, *121*, 1488.
(36) Markiewicz, R. S. *J. Phys. Chem. Sol.* **1995**, *56*, 1637.
(37) O'Brien, M. C. M. *Proc. R. Soc. London, Ser. A* **1964**, *281*, 323.
(38) Riley, M. J.; Hitchman, M. A.; Mohammed, A. W. *J. Chem. Phys.* **1987**, *87*, 3766.
(39) Riley, M. J.; Hitchman, M. A.; Reinen, D. *Chem. Phys.* **1986**, *102*, 11.
(40) Simmons, C. J. *New J. Chem.* **1993**, *17*, 77.
(41) DeMunno, G.; Julve, M.; Nicolo, F.; Lloret, F.; Faus, J.; Ruiz, R.; Sinn, E. *Angew. Chem., Int. Ed.* **1993**, *32*, 613.

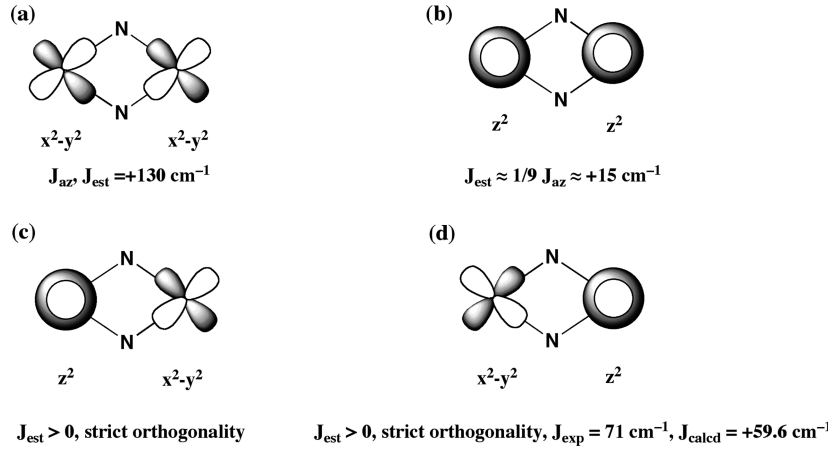

Figure 20. Four possible arrangements (a−d) of the magnetic orbitals in the $[Cu_2(\mu_{1,1}\text{-azido})_2]$ core of **5**. The usual and ideal arrangement coincides with that displayed in a. The experimental (J_{exp}), estimated (J_{est}), and calculated (J_{calcd}) J constants are given in cm^{-1}. The contraction refers to the azido group.

ligands. Taking this into account, the exchange coupling in case d is assumed to be larger than in case e. On the other hand, an antiferromagnetic coupling equivalent to 4/9 of the ideal case is expected for arrangement c. This coupling can also be expressed as a function of the J constants in bipyrimidine (bpm) and oxalate (ox) complexes as follows: $2/9(J_{bpm} + J_{ox})$. It should be noted that these estimations do not consider the changes in the metal−ligand distances. In conclusion, when the ideal orbital topology is lost, a decrease in the magnetic coupling must be observed, independently of whether an axial compressed or an intermediate picture was reached. The DFT calculations show that case e summarizes perfectly the J_1 coupling in **5**, and an intermediate Jahn−Teller distortion cannot be presumed. From these simple concepts, we have obtained an estimated value (−50 cm^{-1}) that is in a good agreement with the value obtained from the experimental data (−34 cm^{-1}). However, a weak ferromagnetic coupling (+9.5 cm^{-1}) is found from DFT calculations due to an underestimation of the antiferromagnetic contributions induced probably by the high negative charge of the used model.

A similar scheme has been done for the J_2 coupling, where uniquely two azido ligands act as bridging ligands (Figure 20). In Figure 20a is shown the ideal case that favors the strong magnetic coupling. As has been demonstrated in a previous work, the magnitude and the nature of this coupling depend on the Cu−N−Cu angle.[31] Taking this into account, a value of +130 cm^{-1} is expected for J_2 in compound **5**. For the case shown in Figure 20b, a net ferromagnetic coupling could be expected, but since the dz^2 orbital shows a lower spin density in the equatorial ring, a decrease in the magnitude of the magnetic coupling must be observed. For the remaining cases, a strict orthogonality takes place and a ferromagnetic coupling is assumed, but its magnitude cannot be easily estimated. One of these latter cases corresponds with J_2 in **5**. DFT calculations are in agreement with the conclusions reached in this section. Thus, even if, just like observed for J_1, there was a shift of the magnitude in our calculations, a moderate ferromagnetic coupling is found (+59.6 cm^{-1}), in agreement with the experimental data (+71 cm^{-1}). The high negative charge in the models used in DFT calculations can lead to problems in the convergence process and to shifts in the values of the J constants. Thus, we think that an underestimation of the antiferromagnetic contributions in J_2 is caused by this fact.

Conclusions

The results reported in this paper clearly show that pyrimidine-2-carboxylato (pymca) is a versatile ligand that is able to afford a rich variety of polynuclear copper(II) complexes with antiferromagnetic magnetic coupling between copper(II) ions. The structure and magnetic properties of the polynuclear copper(II) complexes containing bis(chelating) pymca bridging ligands are strongly influenced by the anion X present in the reaction solution and by the strength of the Cu−X bond. If the X anion lies on the Jahn−Teller distortion axis, as in the case of **2** and **3**, the Cu−X bond is weak, and linear chains with planar pymca−Cu−pymca−Cu fragments are obtained. If X does not act as a bridge and the Cu−X bond is strong, as in the case of **4**, a helical chain is formed, while if the Cu−X bond is strong and the X acts as a bridge, as in the cases of **5** and **7**, the reaction leads to 2D networks.

The bis(chelating) pymca bridging ligand is very effective in transmitting magnetic coupling between copper(II) ions. Thus, if the magnetic orbitals centered on next neighboring copper(II) atoms lie on the plane of the pymca ligand, as in the case of **2**, a strong antiferromagnetic coupling is observed (−276.1 cm^{-1}). It is interesting to note that, despite the structural similarity of complexes **2** and **3**, the J value for the latter is unexpectedly low (−72.5 cm^{-1}). DFT calculations show that the relatively low J value observed for **3** cannot be due to the different configuration of the pymca ligands around the copper(II) ions (cis and trans for **2** and **3**, respectively). The only reasonable explanation for the reduction in the magnetic coupling on passing from **2** to **3** would be the existence of a structural change that places the Jahn−Teller axis pointing at the pymca ligand. Complex **5** represents the first example of a copper(II) complex exhibiting a honeycomb layer in which two pymca bridges alternate with one double end-on azide bridge within the hexagonal rings. Quantum Monte Carlo methods can be successfully

applied to calculate the exchange parameters for the complicated topology observed in **5** with ferromagnetic coupling through the double end-on azide bridges and antiferromagnetic coupling through the pymca bridges. The magnitude of the magnetic coupling in complexes **4**−**7** can be explained on the basis of the overlapping between magnetic orbitals and DFT theoretical calculations. Work is in progress in our laboratory to obtain other homo- and heterometallic pymca-bridged complexes with interesting structures and magnetic properties.

Acknowledgment. This work was supported by the MEC (Spain; Projects CTQ2005/0935 and CTQ2005-08123-C02-02/BQU), the Junta de Andalucía (FQM-195), the University of Granada (grant to A.J.M.), and the Catalan Government (2005SGR-00036).

Supporting Information Available: X-ray crystallographic data in CIF format. Calculated and experimental X-ray powder diffractograms for compounds **1**−**7** (Figure S1), $\pi-\pi$ stacking interaction in compound **5** (Figure S2), magnetic properties of compound **1** (Figure S3), and the theoretical equation used to fit the magnetic data of compounds **1**−**4**. This material is available free of charge via the Internet at http://pubs.acs.org.

IC800625W